Article

Cell

Reactivation of Dormant Relay Pathways in Injured Spinal Cord by KCC2 Manipulations

Graphical Abstract

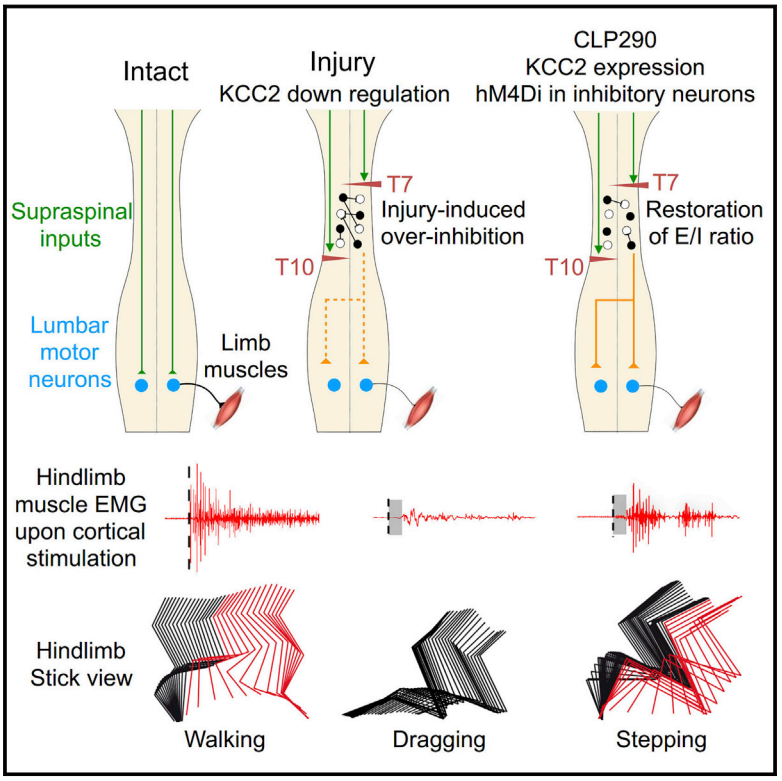

Highlights

- A KCC2 agonist restores stepping ability in paralyzed mice with spinal cord injuries
- KCC2 expression in inhibitory neurons leads to functional recovery
- Restoration of inhibition in injured spinal cord leads to functional recovery

Authors

Bo Chen, Yi Li, Bin Yu, ..., Yiming Zhang, Xiaosong Gu, Zhigang He

Correspondence

nervegu@ntu.edu.cn (X.G.), zhigang.he@childrens.harvard.edu (Z.H.)

In Brief

Reducing the excitability of spinal cord inhibitory interneurons with a small molecule enhances the injured spinal cord's responsiveness to descending inputs and promotes functional recovery after spinal cord injury in mice.

Chen et al., 2018, Cell *174*, 521–535
July 26, 2018
https://doi.org/10.1016/j.cell.2018.06.005

CellPress

Cell

Reactivation of Dormant Relay Pathways in Injured Spinal Cord by KCC2 Manipulations

Bo Chen,[1,4] Yi Li,[1,4] Bin Yu,[2,4] Zicong Zhang,[1] Benedikt Brommer,[1] Philip Raymond Williams,[1] Yuanyuan Liu,[1] Shane Vincent Hegarty,[1] Songlin Zhou,[2] Junjie Zhu,[1] Hong Guo,[3] Yi Lu,[3] Yiming Zhang,[1] Xiaosong Gu,[2,*] and Zhigang He[1,5,*]

[1]F.M. Kirby Neurobiology Center, Boston Children's Hospital, and Department of Neurology, Harvard Medical School, 300 Longwood Avenue, Boston, MA 02115, USA

[2]Key Laboratory of Neuroregeneration of Jiangsu and Ministry of Education, Co-innovation Center of Neuroregeneration, Nantong University, Nantong, 226001 Jiangsu, China

[3]Department of Neurosurgery, Brigham and Women's Hospital, 60 Fenwood Road., BTM 4th Floor, Boston, MA 02115, USA

[4]These authors contributed equally

[5]Lead Contact

*Correspondence: nervegu@ntu.edu.cn (X.G.), zhigang.he@childrens.harvard.edu (Z.H.)

https://doi.org/10.1016/j.cell.2018.06.005

SUMMARY

Many human spinal cord injuries are anatomically incomplete but exhibit complete paralysis. It is unknown why spared axons fail to mediate functional recovery in these cases. To investigate this, we undertook a small-molecule screen in mice with staggered bilateral hemisections in which the lumbar spinal cord is deprived of all direct brain-derived innervation, but dormant relay circuits remain. We discovered that a KCC2 agonist restored stepping ability, which could be mimicked by selective expression of KCC2, or hyperpolarizing DREADDs, in the inhibitory interneurons between and around the staggered spinal lesions. Mechanistically, these treatments transformed this injury-induced dysfunctional spinal circuit to a functional state, facilitating the relay of brain-derived commands toward the lumbar spinal cord. Thus, our results identify spinal inhibitory interneurons as a roadblock limiting the integration of descending inputs into relay circuits after injury and suggest KCC2 agonists as promising treatments for promoting functional recovery after spinal cord injury.

INTRODUCTION

Most human spinal cord injuries (SCIs) are anatomically incomplete, with spared axons spanning the damaged spinal segments. However, about a half of these patients have a total loss of muscle control and sensation below the injury level (Fawcett et al., 2007; Kakulas, 1999), suggesting that spared connections are functionally dormant. Remarkably, recent studies have demonstrated that epidural stimulation combined with rehabilitative training allows some chronically paralyzed patients with a SCI to regain voluntary movement (Angeli et al., 2014; Harkema et al., 2011). A postulated mechanism is that these manipulations reactivate dormant spinal circuitry, enabling brain-derived signals to be relayed to the spinal cord. However, it is largely unknown why this spared spinal circuitry is dysfunctional after SCI and how it can best be reactivated.

In the case of hindlimb function, the spinal center for executing basic locomotion, the central pattern generator (CPG), is primarily located in the lumbar spinal cord (Frigon and Rossignol, 2008; Gerasimenko et al., 2008; Grillner and Wallén, 1985; Kiehn, 2016). Classical studies, using spinal cords isolated from neonatal animals, showed that pharmacological manipulations of neuronal excitability could initiate and modulate the efferent patterns (Cazalets et al., 1992; Cowley and Schmidt, 1995; Kiehn, 2006). In intact animals, the output of the lumbar locomotor center is controlled, in part, by descending commands from the brain. After being deprived of these inputs by SCI, the lumbar spinal cord fails to initiate locomotor function, even when sensory afferents are intact. To restore function after SCI, it is crucial to re-establish the connections between descending inputs and the lumbar spinal cord. For example, compensatory axon regrowth and synapse reorganization could enhance such connections at different spinal levels after SCI (Ballermann and Fouad, 2006; Bareyre et al., 2004; Courtine et al., 2008; Filous and Schwab, 2018; He and Jin, 2016; Jankowska and Edgley, 2006; Rosenzweig et al., 2010; Takeoka et al., 2014; van den Brand et al., 2012; Zaporozhets et al., 2011). In severe spinal cord injury in which the majority of descending spinal-projecting pathways are damaged, the engagement of intraspinal networks, consisting of local interneurons limited to single spinal segments and projecting propriospinal neurons whose axons cross many spinal segments, can function as indirect relay pathways to receive and transmit brain-derived motor commands to the lumbar spinal cord (O'Shea et al., 2017; Zaporozhets et al., 2011).

Different hypotheses have been put forward to explain why spared connections have a limited ability to compensate after SCI. For example, the firing and conduction properties of neurons with spared descending axons could be compromised (Edgerton et al., 2008; Arvanian et al., 2009; Sawada et al., 2015). Alternatively, local spinal cord circuits could be rendered

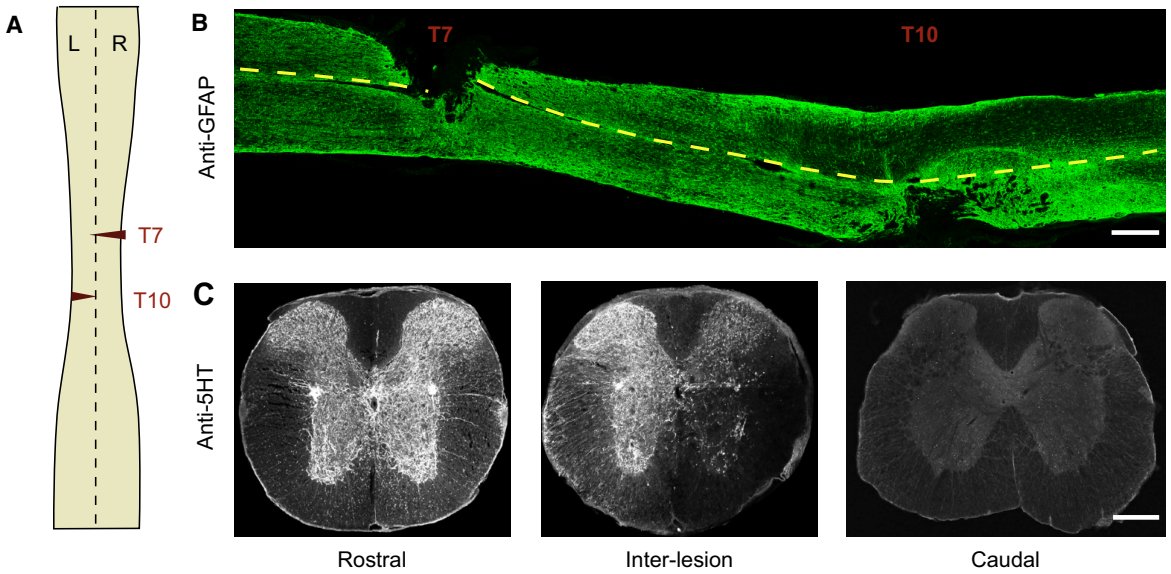

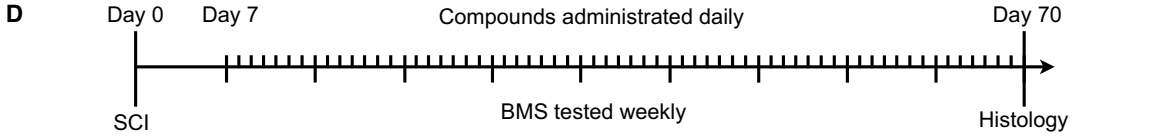

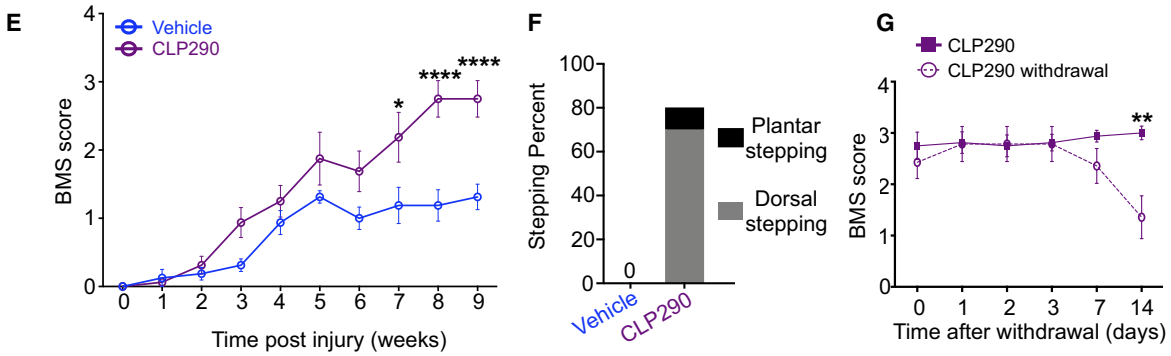

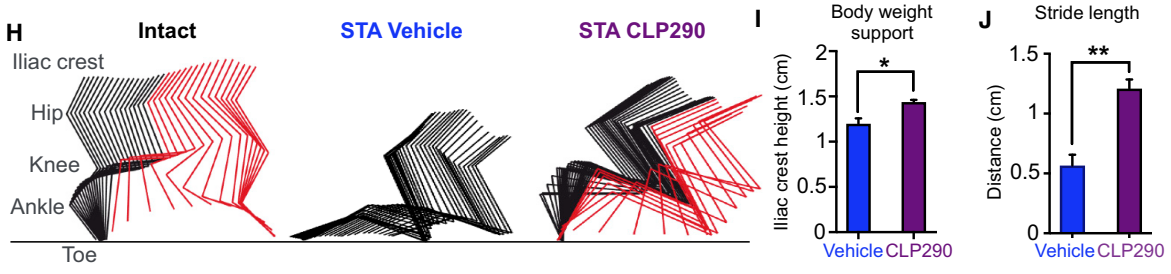

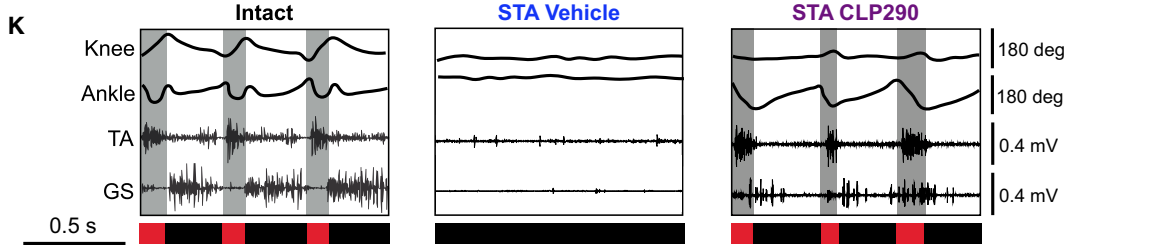

(legend on next page)

non-functional by injury, such that they may no longer be able to relay or integrate the spared descending inputs (Courtine et al., 2008; Edgerton et al., 2008; Rossignol and Frigon, 2011). The contribution of these and other factors remains to be characterized. Moreover, it is not even clear whether inhibiting or enhancing the excitability of spared spinal neurons would be beneficial for functional recovery after SCI.

Remarkable progress has been made in characterizing the cellular and molecular mechanisms regulating neuronal excitability. As a result, a number of small-molecule compounds have been developed to target key regulators, such as ion channels and receptors, and their pharmacological properties have been well characterized. Importantly, many of these compounds can efficiently cross the blood-brain barrier (BBB), and, doing so, enables the systemic administration of these small molecules to analyze their effects in SCI animal models. Thus, we decided to take a non-biased compound screening approach to identify neuronal activity modulators that can reactivate dormant spinal circuitry and, ultimately, mediate functional recovery in SCI models.

RESULTS

CLP290 Restores Consistent Stepping Ability in Paralyzed Mice with Staggered Lesions

We first optimized a staggered lesion paradigm in which two lateral hemisections were performed at the thoracic (T) 7 and T10 levels simultaneously (Figures 1A and 1B), similar to the model previously described (Courtine et al. 2008; van den Brand et al., 2012). The T10 lesion is a lateral hemisection that ends at the spinal cord midline, while the T7 lesion, contralateral to the T10 lesion, extends slightly beyond the midline (Figure 1A). With this double hemisection procedure, all descending axons passing T10 are severed, leaving only those crossing the midline between T7 and T10 intact (Figure 1C). Indeed, by immunohistochemistry with anti-5-HT antibodies, which label serotonergic axons, descending serotonergic axons could be detected in the spinal cord segments between the lesions, but not in the lumbar spinal cord (Figure 1C). Thus, a relay zone remains between and around the lesions (T7 and T10), where descending axons terminate and where some propriospinal neurons maintain their connections with lumbar spinal neurons (see below).

The mice with this staggered lesion exhibited nearly complete and permanent hindlimb paralysis (Figures 1E and 1F). During the 10 weeks after injury, injured mice rarely showed ankle movement and never displayed any type of stepping, with a score of 0.5 or 1 on the Basso mouse scale (BMS), an established open-field locomotion test (Basso et al., 2006). Thus, the spared relay pathways between T7 and T10 must remain dormant.

We used this double hemisection SCI model to seek small-molecule compounds that could reactivate the spared, but dormant, spinal connections by monitoring hindlimb motor performance during overground locomotion. To this end, we started daily compound treatment 1 week after injury, and then monitored the BMS scores approximately 24 hr after the previous day's compound treatment on a weekly basis (Figure 1D). Behavioral outcomes observed at these time points likely reflect sustained effects of the treatment, which are more clinically relevant.

Candidate compounds were chosen based on their ability to modulate neuronal excitability upon systemic delivery. They included baclofen, a GABA receptor agonist; bumetanide, an inhibitor of the $Na^+/2Cl^-/K^+$ co-transporter (NKCC1); CLP290, an agonist of the neuron-specific K^+-Cl^- co-transporter (KCC2), also called SLC12A5; L838,417, a $GABA_A$-positive allosteric modulator; CP101606, an NMDA receptor antagonist; 8-OHDPAT, a 5HT1A/7 agonist; and quipazine, a 5HT2A/C agonist (Figures 1E and S1A). None of these treatments resulted in significant improvements in stepping ability within the first 2–3 weeks after daily treatment. However, in CLP290-treated mice, functional recovery first appeared by 4–5 weeks and became significant from 7 weeks after treatment (Figure 1E). Bumetanide also showed some effects, but without statistical significance (Figure S1A). Thus, our further analyses focused on CLP290-treated SCI mice.

The majority (80%) of CLP290-treated mice recovered consistent hindpaw plantar placement and weight-bearing stepping (most with dorsal stepping and some with plantar stepping)

Figure 1. Identification of CLP290 as a Compound Leading to Functional Recovery in Mice with Staggered Lesions

(A) Schematic of staggered lateral hemisections at T7 and T10. Arrowheads indicate lesions; L, left; R, right.

(B) Representative image of an anti-GFAP-stained spinal cord section 10 weeks after overstagger lesion. Dashed line indicates midline. Scale bar, 500 μm.

(C) Representative image stacks of anti-5HT-stained transverse sections from T5 (rostral to lesions), T8 (between lesions), and L2 (caudal to lesions) of mice at 2 weeks after staggered lesions. Scale bar, 100 μm.

(D) Experimental scheme. Each BMS test was performed 24 hr prior to daily compound treatment.

(E) BMS scores in injured mice with continuous treatment of CLP290 (35 mg/kg) and vehicle solution. Two-way repeated-measures ANOVA, followed by post hoc Bonferroni correction. Both groups started as n = 10, and, at week 9 (the termination time point), were n = 8 and n = 10 for the vehicle and CLP290, respectively. *$p < 0.05$; ****$p < 0.0001$. Error bars, SEM.

(F) Percentage of mice that reached stepping. CLP290 versus vehicle at 9 weeks post-staggered injury (n = 8 and n = 10 for the vehicle and the CLP290 group, respectively).

(G) Sustained behavioral improvements after CLP290 withdrawal in mice with 10-week treatment. BMS was tested on days 1, 2, 3, 7 and 14 after compound withdrawal (n = 7). Two-way repeated-measure ANOVA, followed by post hoc Bonferroni correction. **$p < 0.01$. Error bars, SEM.

(H) Color-coded stick view decomposition of mouse right hindlimb movements during swing, stance (intact group), dragging (vehicle group), and stepping (CLP290 group).

(I and J) Quantification of bodyweight support (I) and stride length (J) of mice at 9 weeks post-staggered injury (n = 8 and n = 10 for the vehicle and the CLP290 group, respectively). Student's t test (two-tailed, unpaired). *$p < 0.05$; **$p < 0.01$. Error bars, SEM.

(K) Representative right hindlimb knee and ankle angle oscillation trace and simultaneous EMG recording from *tibias anterior* (TA) and *gastrocnemius medialis* (GS) muscles. Black bars, swing and stepping; red bars, stance and dragging.

See also Figures S1, S2, and S3 and Video S1.

(Figure 1F; Video S1), in contrast to control mice and mice treated with other compounds, which predominantly demonstrated paralyzed hindlimbs. This extent of recovery is functionally significant, as stepping ability has been implicated as the limiting step for functional recovery in severe injury models (Schucht et al., 2002). During stepping, CLP290-treated mice could partially support their body weight and exhibited significantly increased oscillation of hindlimb joints (Figures 1H–1K). By electromyogram (EMG) recording in injured control mice (Figure 1K), we found that the ankle flexor *tibialis anterior* (TA) muscle was rarely active, while activity of the extensor *gastrocnemius soleus* (GS) muscle was never observed. In contrast, CLP290-treated mice showed both TA and GS activity (Figure 1K). Consequently, the total hindlimb stride length in CLP290-treated mice was significantly increased (Figure 1J). Intriguingly, different from intact mice, which have alternating activation of TA (swing phase) and GS (stance phase) during stepping gait, CLP290-treated SCI mice showed co-activation of TA and GS during the swing phase (Figure 1K), a sign of suboptimal bodyweight support.

Further, in mice with CLP290-induced recovery, the BMS scores remained significantly higher than those for controls for 1–2 weeks after stopping treatment (Figure 1G), suggesting that sustained functional recovery resulted from CLP290 treatment. At the end of these experiments, we observed no immunostaining with the anti-5-HT antibody in the lumbar region and verified the success of staggered lesions in these mice (Figure S1C). Together, our results demonstrate that CLP290 treatment enables most paralyzed mice to restore weight-bearing stepping capacity in a sustained fashion.

CLP290 Treatment Does Not Induce Functional Improvement in Mice with Complete Lesions

CLP290's effects could result from reactivating the spared dormant descending connections in the spinal cord after SCI. However, it could also directly act on the lumbar spinal cord independent of the descending inputs. To distinguish between these possibilities, we applied the same CLP290 treatment to mice with a complete T8 spinal cord transection, in which no axons cross the lesion site (Figure S1D), and found that CLP290 failed to promote any significant functional recovery (Figures S1E). Conversely, the 5-HT receptor agonist quipazine led to a rapid, but transient, BMS improvement (starting at 10 min and lasting for less than 2 hr) in both the staggered lesion (Figure S1B) and the T8 complete transection models (Figure S1F). Therefore, different from this transient effector that directly acts on the lumbar spinal cord, the effects of CLP290 on functional improvement are dependent on spared connections.

CLP290 Does Not Affect Axon Regrowth

Previous studies have shown that CLP290 can alleviate neuropathic pain in a peripheral nerve injury model (Gagnon et al., 2013), while injury-induced KCC2 downregulation has been associated with SCI-related spasticity (Boulenguez et al., 2010; Côté et al., 2014). As mice with either staggered lesions or complete lesions display similar SCI-associated behavioral deficits (pain and spasticity), our results showing that CLP290 induces functional recovery in mice with staggered lesions only suggest that the functional improvements of CLP290 are likely independent of such analgesic and anti-spastic effects. Thus, the possible mechanisms for CLP290 are likely to rely on the spared relay pathway, for example, by promoting axonal sprouting and/or by increasing the fidelity of the relay pathway signal to the lumbar spinal cord.

To test these possibilities, we first asked whether CLP290 increased the regrowth of spared propriospinal axons, and/or their connecting axons from the brain. To analyze neuronal projections to the hindlimb locomotor control center in each condition, we injected a retrograde tracing pseudotyped lentiviral vector (HiRet) expressing mCherry (HiRet-mCherry) (Kato et al., 2011; Wang et al., 2017; Liu et al., 2017) into the lumbar enlargement (L2–L4). At 2 weeks after injury, most retrogradely labeled neurons were found in the spinal cord segments between and around the lesions, with few above the lesion and none in the brain (Figure S2). The number of retrogradely traced neurons in the spinal cord increased by 10 weeks after injury, consistent with previous reports (Courtine et al., 2008), but CLP290 treatment did not affect these measures (Figures S2C and S2F). Similarly, anterograde tracing from the brain with AAV-ChR2-mCherry and AAV-ChR2-GFP, failed to reveal increased sprouting of descending brainstem reticulospinal axons (Figures S3A–S3C), or corticospinal axons (Figures S3G–S3I), in the spinal cords of CLP290-treated mice at 2 and 10 weeks after injury. Similarly, the sprouting of serotonergic axons detected by 5-HT immunohistochemistry was also not affected by CLP290 treatment (Figures S3D–S3F). Thus, it is unlikely that CLP290 acts by promoting the regrowth of brain-derived descending axons into the relay zone or propriospinal axons projecting to the lumbar spinal cord.

KCC2 Expression Mimics the Effects of CLP290 to Promote Functional Recovery

CLP290 was identified as an activator of the K^+-Cl^- co-transporter KCC2, but it may also act on other targets (Gagnon et al., 2013). Thus, we asked whether overexpression of KCC2 in CNS neurons had effects similar to that of CLP290 in staggered-lesioned mice. Taking advantage of AAV-PHP.B vectors that can cross the BBB in adult mice (Deverman et al., 2016), we injected AAV-PHP.B-expressing KCC2 under control of the human synapsin promoter (AAV-PHP.B-syn-HA-KCC2) into the tail vein. We performed injections directly after injury because KCC2 took 1-2 weeks to be detectably expressed. We then performed weekly behavioral monitoring (Figure 2A). As shown in Figure 2B, AAV-PHP.B-KCC2 treatment resulted in widespread expression of HA-tagged KCC2 in all spinal cord segments as analyzed 8 weeks post-injury. In contrast to control AAV-PHP.B-H2B-GFP, AAV-PHP.B-KCC2 treatment led to significant functional recovery (Figures 2C–2H), to an extent similar to or greater than CLP290 (Figures 1E –1J). Indeed, at 8 weeks after AAV-KCC2 treatment, 80% of these mice were able to step with ankle joint movement involving TA and GS, and about a half of these mice could achieve plantar stepping with both ankle and knee movements (Figures 2D and 2H). Furthermore, AAV-KCC2-treated mice could partially support their body weight with frequent GS firing during the stance phase (Figures 2E and H).

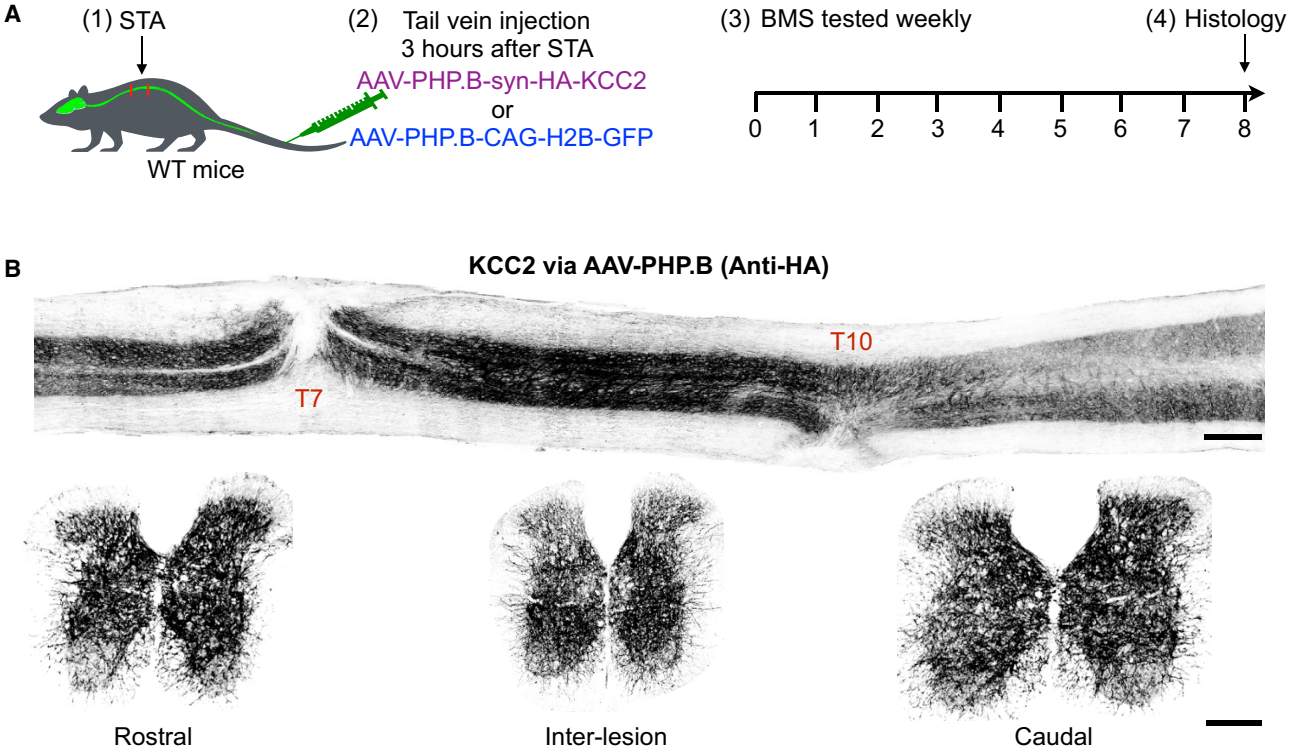

(legend on next page)

At the termination of this experiment (9–10 weeks after injury), we analyzed the expression levels of KCC2 in the spinal cord by western blotting. In control mice, KCC2 is significantly reduced in the lumbar and inter-lesion spinal cord segments after injury (Figures S4A and S4B), consistent with previous reports (Boulenguez et al., 2010; Côté et al., 2014). However, AAV-KCC2 treatment restored KCC2 expression to levels significantly closer to uninjured mice relative to AAV-GFP controls (Figures S4A and S4B). Thus, AAV-KCC2 likely acts by counteracting SCI-induced KCC2 downregulation.

Selective KCC2 Expression in Inhibitory Interneurons Leads to Functional Recovery

We next assessed whether KCC2 expression in specific types of neurons accounts for the observed functional recovery. To do this, we injected AAV-PHP.B-FLEX-KCC2 (Cre-dependent KCC2 expression) into the tail vein of adult mice of Vglut2-Cre (for excitatory neurons) (Tong et al., 2007), Vgat-Cre (for inhibitory neurons) (Vong et al., 2011), or Chat-Cre (for motor neurons and a subset of interneurons) (Rossi et al., 2011) directly after injury (Figures 3A and 3B). In contrast to Chat-Cre and Vglut2-Cre mice, Vgat-Cre mice injected with AAV-PHP.B-FLEX-KCC2 showed significant functional recovery (Figures 3C–3E), to an extent similar to CLP290 treatment (Figure 1) or non-selective KCC2 expression (Figure 2). Thus, our results suggest that KCC2 dysfunction or downregulation in inhibitory interneurons limits hindlimb functional recovery in staggered-lesioned mice.

KCC2 Acts through Inhibitory Interneurons in the Spinal Cord Segments between and around the Staggered Lesions to Induce Functional Recovery

As shown in Figures S2 and S3, propriospinal neurons in the relay zone, consisting of the spinal cord segments between and below the staggered lesions, are likely to relay the brain-derived signals to the lumbar spinal cord. Thus, there are two possible mechanisms for KCC2-mediated hindlimb functional recovery in stagger-lesioned mice: (1) KCC2 acts on the inhibitory interneurons in the lumbar segments (L2–L5) to facilitate the integration of propriospinal inputs, and/or (2) KCC2 acts on the inhibitory neurons in the relay zone above the lumbar spinal cord to facilitate the integration of brain-derived inputs from descending pathways, and/or its relay to the lumbar spinal cord.

To test these possibilities, we injected AAV-KCC2 or AAV-FLEX-KCC2 locally into lumbar segments (L2–L5) of wild-type mice or Vgat-Cre mice (Figures 4A, 4B, and S4C). These treatments did not lead to significant functional recovery (Figures 4C and 4D), suggesting that the inhibitory neurons in the lumbar spinal cord are unlikely to mediate the functional recovery effects of KCC2.

To introduce KCC2 into spinal cord segments between and around the staggered lesions, we took advantage of the compromised blood-spinal cord-barrier around the lesion sites acutely after the injury. We injected AAV-KCC2 or AAV-FLEX-KCC2 into the tail vein of wild-type or Vgat-Cre mice, respectively, at 3 hr after overstaggered lesions (Figure 4E). As a result, KCC2 expression spanned between T5 and T12 (Figures 4F and S4D). In these animals, we observed a significant and persistent functional recovery, with increased BMS performance, in both groups of mice (Figures 4G and 4H), to extents comparable to AAV-PHP.B-KCC2 treatment (Figure 2). In these Vgat-Cre mice with AAV-FLEX-KCC2, accompanying CLP290 treatment did not significantly enhance functional recovery at most time points (Figure S4E), consistent with the notion that the effects of CLP290 were mainly mediated by activating KCC2 in these inhibitory interneurons. Thus, KCC2/CLP290 primarily acts on inhibitory neurons in the relay zone, between and adjacent to the lesion sites in thoracic spinal cord levels, to facilitate hindlimb functional recovery.

CLP290/KCC2 Alters Excitability and Relay Formation

In mature neurons, GABA and glycine are inhibitory because they open chloride channels, which allow chloride ion influx leading to hyperpolarization. In contrast, during development, the elevated intracellular chloride levels render $GABA_A$- and glycine-mediated currents depolarizing and generally excitatory. During early postnatal life, KCC2 upregulation in postnatal neurons is crucial for reducing intracellular chloride concentrations, transforming excitation into inhibition (Ben-Ari et al., 2012; Kaila et al., 2014). Thus, injury-induced KCC2 downregulation (Boulenguez et al., 2010; Côté et al., 2014) would be expected to restore an immature state in which GABA and glycine receptors can depolarize neurons. In this scenario, KCC2 activation in spinal inhibitory neurons would transform local circuits in the relay zone toward a more physiological state, which is more receptive to descending inputs. To examine this, we used c-Fos immunoreactivity as a proxy of neuronal activity in the spinal cord segments between T7 and T10 at 8 weeks after injury, and after walking on a treadmill for 1 hr. In each group, the majority

Figure 2. Widespread KCC2 Expression Mimics the Effects of CLP290 to Promote Functional Recovery

(A) Experimental scheme.

(B) Representative image stacks of longitudinal (upper) and transverse (lower) spinal cord sections, taken from the mice at 8 weeks after staggered injury, stained with anti-HA (to detect the HA-KCC2 protein). Scale bar, 500 (upper) and 100 μm (lower).

(C) BMS performance in experimental (AAV-PHP.B-HA-KCC2) and control (AAV-PHP.B-H2B-GFP) groups. Two-way repeated-measures ANOVA followed by post hoc Bonferroni correction. *$p < 0.05$. Error bars represent SEM.

(D) Percentage of mice that reached stepping at 8 weeks after injury.

(E and F) Quantification of bodyweight support (E) and stride length (F) at 8 weeks ($n = 10$ per group). Student's t test (two-tailed, unpaired) was applied. *$p < 0.05$; **$p < 0.01$. Error bars, SEM.

(G) Color-coded stick view decomposition of mouse right hindlimb movement during dragging (AAV-PHP.B-H2B-GFP group) and stepping (AAV-PHP.B-HA-KCC2 group).

(H) Representative right hindlimb knee and ankle angle oscillation trace and simultaneous EMG recording of mice at 8 weeks after injury. Red bars, swing and stepping; black bars, stance and dragging.

See also Figure S4 and Video S1.

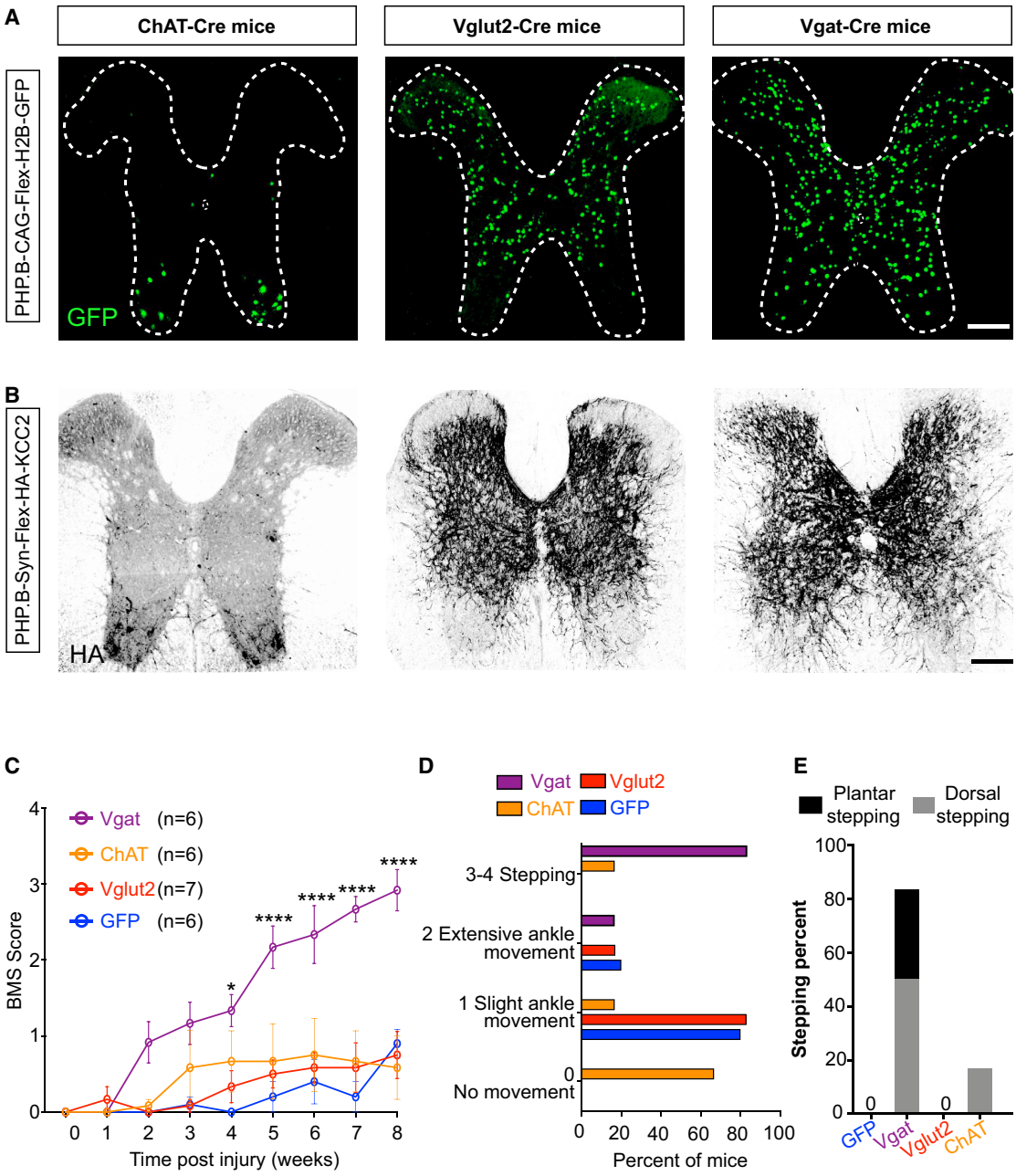

Figure 3. KCC2 Expression in Inhibitory Neurons Leads to Functional Recovery

(A and B) Representative image stacks showing expression of GFP (A) or HA-KCC2 (B) in T8 spinal cord of indicated transgenic mice with tail-vein injection of AAV-PHP.B-CAG-Flex-H2B-GFP (A) or AAV-PHP.B-Syn-Flex-HA-KCC2 (B). Scale bar, 100 μm.

(C) BMS performance in indicated groups. Two-way repeated-measure ANOVA followed by post hoc Bonferroni correction. *$p < 0.05$; ****$p < 0.0001$. Error bars, SEM.

(D) Breakdown of BMS scores for indicated treatment groups at 8 weeks after injury.

(E) Percentage of mice that reached plantar or dorsal stepping at 8 weeks after injury.

of c-Fos-positive cells in these spinal segments were also positively stained with NeuN, a neuronal marker (Figures S5A and S5B). Representative composites of c-Fos/NeuN double-positive cells are shown in Figure 5A. In injured mice without treatment, the c-Fos-positive neurons were concentrated in the dorsal horn of the spinal cord (Figures 5A–5C), perhaps reflecting hypersensitivity to peripheral sensory inputs in these injured mice. With CLP290 or AAV-KCC2 treatment, the distribution of c-Fos-positive neurons became very different, with a reduction in the dorsal horn (laminae I–V), and a significant

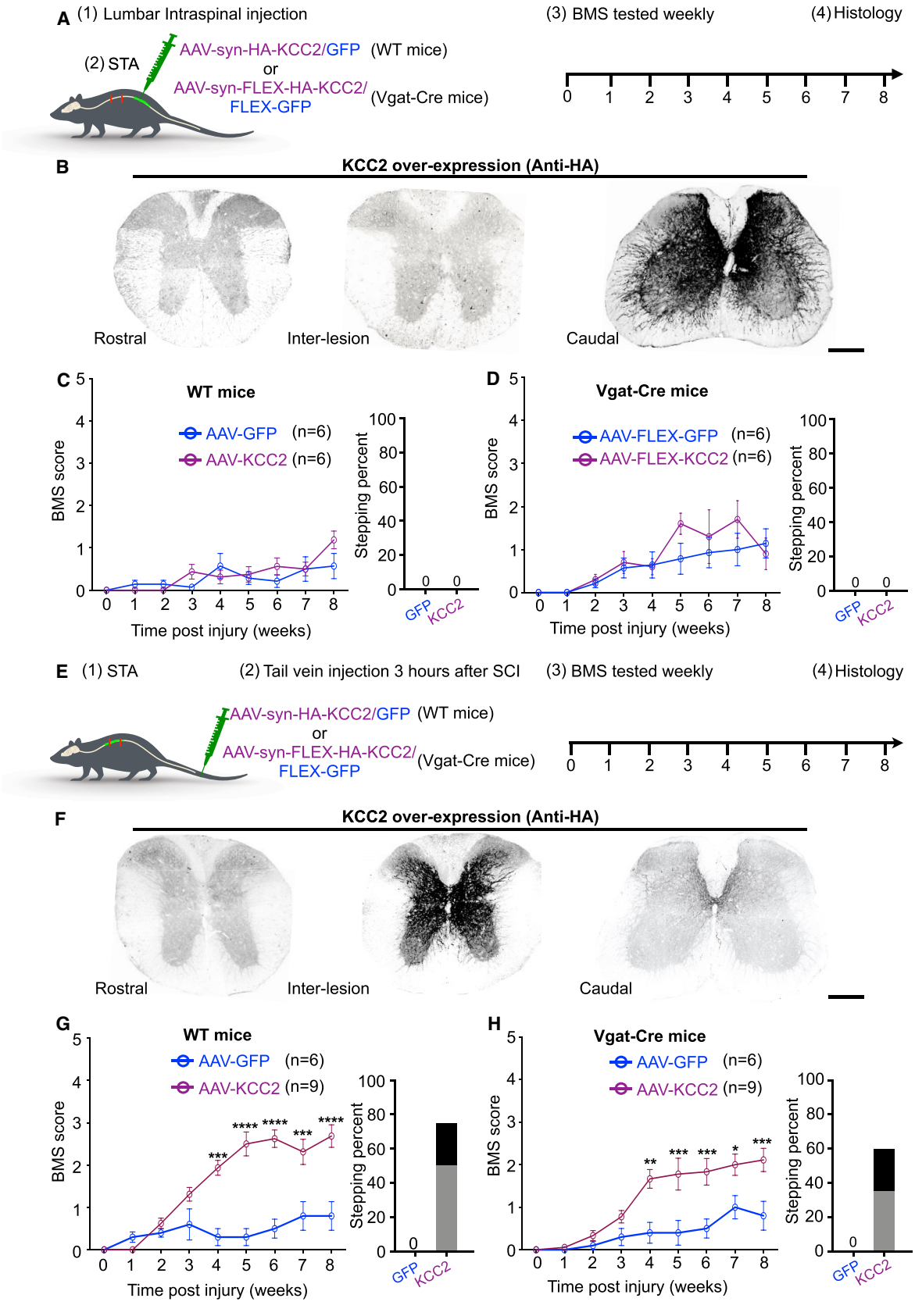

(legend on next page)

increase in the intermediate and ventral spinal cord (Figures 5A–5C). This KCC2-transformed distribution pattern is similar to what was detected in intact mice, in response to walking (Figures 5A–5C). 2 weeks after withdrawal of CLP290 treatment, the c-Fos pattern returned to what seen without treatment (Figures S5C and S5D), consistent with the behavioral outcomes (Figure 1G). Taken together, these findings suggest that increasing KCC2 activity restores a more physiological neuronal activity pattern to the local spinal cord circuitry.

As a control, we examined c-Fos immunoreactivity in the spinal cord of staggered injured mice following chronic treatment with L838,417, a GABA agonist that has been shown to reduce neuropathic pain (Knabl et al., 2008). As shown in Figures 5A and 5B, L838,417 reduced c-Fos-positive neurons in dorsal horn, but without increasing those in intermediate zones and ventral region, corroborating the results that L838,417 treatment failed to promote functional motor recovery (Figure S1A). As the intermediate and ventral spinal cord are major termination zones of descending inputs, increased neuronal activity in this area after CLP290/KCC2, but not L838,417, treatment likely reflects improved responses to descending inputs. Thus, these results suggest that chronic KCC2/CLP290 treatment transform the SCI-induced, sensory-centralized activation pattern of the relay zone, into a state under control of both sensory and descending pathways.

To test directly whether the treated spinal cord could more efficiently relay descending inputs to the lumbar spinal cord, we performed cortical stimulation and recorded EMG responses in the TA muscle (Figure 5D). The latency of the cortical-stimulating response was significantly delayed in SCI mice compared to intact mice, and KCC2-related treatments failed to shorten the latency of the stimulation response (Figures 5D and 5E). These results are consistent with the notion that multiple synaptic connections exist in the KCC2-activated circuitry, which relays cortical stimulation to the motor neurons in the lumbar cord of injured mice. On the other hand, the amplitude of evoked EMG signals was significantly increased in injured mice with AAV-PHP.B-syn-HA-KCC2 or CLP290 treatment, compared to controls (Figures 5D and 5F), suggesting that KCC2 enhanced the relay efficiency of this spinal circuitry. Thus, KCC2 treatment facilitates the transmission of descending inputs from the brain to the lumbar spinal cord.

DREADD-Assisted Modulation of Inhibitory Neuron Excitability Mimics the Effects of KCC2/CLP290

To test if reducing the excitability of inhibitory interneurons could mimic the effects of KCC2 and CPL290, we expressed hM4Di-mCherry, an inhibitory Gi-coupled receptor Gi-DREADD (Krashes et al., 2011), in inhibitory interneurons between and the around lesion by injecting AAV9 vectors (AAV9-FLEX-hM4Di-mCherry or AAV9-GFP) into the tail vein of Vgat-Cre mice 3 hr after injury (Figure 6A). We administered clozapine N-oxide (CNO), which selectively activates Gi-DREADD (Roth, 2016), daily and monitored behavior weekly. When tested at 24 hr after CNO administration (using the same treatment schedule as for CLP290), we found that injured mice with hM4Di, but not GFP, showed a similar degree of sustained functional recovery as observed with CLP290 or KCC2 treatment (Figure 6C). Furthermore, hM4Di- and CNO-treated mice exhibited c-Fos expression patterns similar to that observed with KCC2-related treatments after continuous walking (Figures 5A and 6D–6F). Thus, these results verified the beneficial effects of reducing the excitability of inhibitory interneurons.

Considering that overall disinhibition within the inter-lesion segments of SCI mice via hM4Di, and the KCC2-related treatments, could increase the activity of excitatory neurons, we asked if direct activation of excitatory interneurons could mimic the effects of inhibiting inhibitory interneurons. AAV9-GFP or AAV9-FLEX-hM3Dq-mCherry were injected to the tail vein of Vglut2-Cre mice right after staggered lesions (Figure S6A). As shown in Figure S6B, expression of this depolarizing hM3Dq in excitatory spinal neurons (AAV9-FLEX-hM3Dq-mCherry into Vglut2-Cre), combined with daily CNO delivery, failed to elicit functional recovery within 8 weeks of daily CNO treatment. Intriguingly, immediately after CNO administration, there was a transient functional improvement, but with hindlimb spasticity (Figure S6C; data not shown), that is similar to what was seen after quipazine treatment (Figure S1B). Thus, directly reducing the excitability of inhibitory interneurons, but not directly increasing the excitability of excitatory interneurons, in the spinal cord is a powerful strategy to enhance responsiveness to descending inputs, and to ultimately promote lasting functional recovery after severe SCI.

DISCUSSION

Using a bilateral hemisection model removing all supraspinal descending connections to the lumbosacral spinal cord, we demonstrated that chronic KCC2 activation, either pharmacologically or through AAV-assisted gene delivery, reactivates dormant spared circuitry and results in persistent hindlimb stepping. Inhibitory interneurons in the spinal cord segments between the lesions and above the lumbar spinal cord primarily mediate this effect. We propose that by counteracting

Figure 4. KCC2 Acts on Inhibitory Neurons in the Spinal Cord Segments between and around Lesions

(A) Experimental scheme for (B)–(D).

(B) Representative images of anti-HA-stained transverse sections of the thoracic and lumbar spinal cord at 8 weeks. Scale bar, 100 μm.

(C and D) Left: BMS performance in different treatment groups in wild-type mice (C) and Vgat-Cre mice (D). Right: percentage of mice that reached stepping in WT mice (C) and Vgat-Cre mice (D). ANOVA followed by post hoc Bonferroni correction. Error bars, SEM.

(E) Experimental scheme for (F)–(H).

(F) Representative images of anti-HA-stained transverse sections of the thoracic and lumbar spinal cord at 8 weeks after injury. Scale bar, 100 μm.

(G and H) Left: BMS performance in experimental and control groups in WT mice (G) and Vgat-Cre mice (H). Right: percentage of mice that reached stepping in WT mice (G) and Vgat-Cre mice (H). ANOVA followed by post hoc Bonferroni correction. *$p < 0.05$. Error bars, SEM.

See also Figure S4.

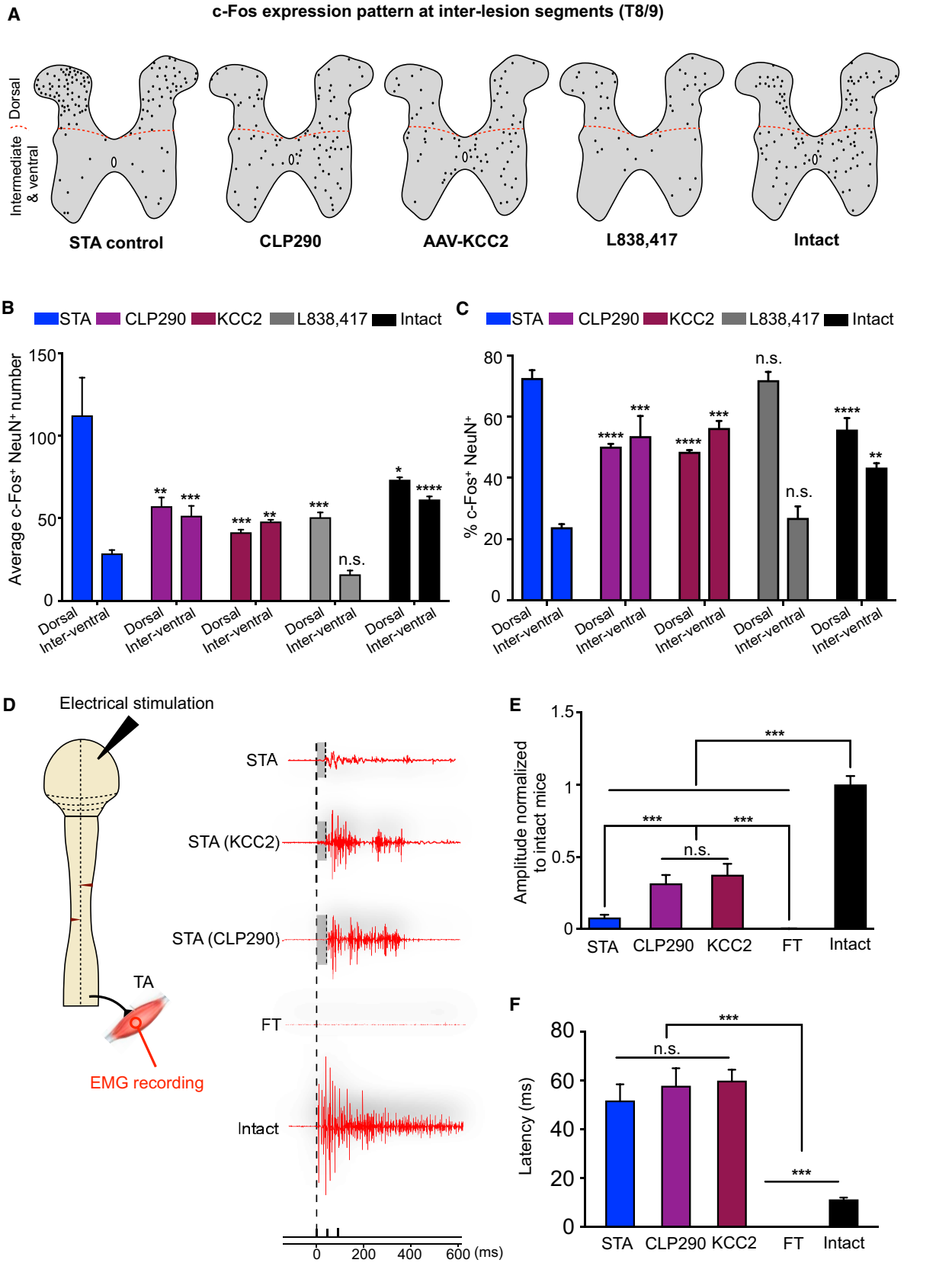

(legend on next page)

injury-induced KCC2 downregulation, these treatments modulate neuronal excitability in the relay zone, reanimating spinal circuits that had been rendered non-functional by injury. As a result, these local circuits are better able to relay commands from descending projections to the lumbar spinal cord, resulting in improved behavioral recovery.

Mechanistic Differences and Relevance to Other Treatments

Previous studies showed that even in complete thoracic SCI, pharmacological approaches, such as serotonergic and dopaminergic agonists and antagonists of GABA/glycine receptors, can induce immediate, but transient, hindlimb locomotion (Courtine et al., 2009; de Leon et al., 1999; Edgerton et al., 2008; Robinson and Goldberger, 1986; Rossignol and Barbeau, 1993). Because the lumbar spinal cord is completely disconnected from the brain in these "spinal animals," pharmacological treatments likely act by altering the excitability of the spinal circuitry, enabling it to respond to only sensory inputs. Consistently, we found that serotonergic agonists induced acute, but only transient locomotion (for up to 2–3 hr after compound administration), with no sustained improvements in both complete and staggered lesion models. In contrast, CLP290 induced sustained functional recovery in mice with staggered but not complete lesion. Thus, while serotonergic modulators likely act on local sensory-driven circuits in the lumbar spinal cord, CLP290 recruits dormant spared connections from the brain after SCI.

In addition, the combinatorial treatment of epidural stimulation and rehabilitation also has been shown to induce some degree of voluntary movement in rats with staggered lesions (together with a pharmacological cocktail of serotonergic and dopaminergic agonists) (van den Brand et al., 2012) and in some chronic SCI patients (Angeli et al., 2014; Harkema et al., 2011). While extensive axonal sprouting has been observed in these rats (van den Brand et al., 2012), it is unknown whether axon sprouting is causally related to the functional improvements. Recent studies suggest that electrical neuromodulation applied to the dorsal aspect of lumbar segments primarily engages proprioceptive feedback circuits (Capogrosso et al., 2013; Hofstoetter et al., 2015; Wenger et al., 2014). However, it remains unknown how this leads to functional restoration of descending input-dependent voluntary movement. In light of our results showing that reducing the excitability of inhibitory interneurons in the relay zone above the lumbar spinal cord is sufficient to enable this spinal circuitry to relay brain-derived commands to the lumbar spinal cord, it would be interesting to test whether epidural stimulation and/or combined treatments also engage with inhibitory interneurons to mediate their functional effects.

KCC2 and Rebalancing Spinal Locomotor Circuitry

Injury triggers a battery of alterations in the spinal cord, such as local KCC2 downregulation. Our results suggest that reactivation of KCC2 in inhibitory interneurons may re-establish the excitation/inhibition (E/I) ratio across the spinal network following SCI. This is consistent with the notion that inhibitory input is critical not only for sculpting specific firing patterns within a neural network but also for preventing network activity from becoming dysfunctional (Möhler et al., 2004). Importantly, not all inhibition-enhancing manipulations are effective. In contrast to KCC2 or Gi-DREADD, GABA receptor agonists appear to reduce the overall activation patterns across the spinal cord, but fail to re-establish more physiological activation patterns, or to promote functional improvements. This could be due to its direct and non-selective inhibition, as L838,417 treatment reduced neuronal activation levels in all spinal cord regions, including crucial ventral motor associated laminae, which is expected to decrease the quality of motor control overall. Finally, direct excitation of spinal excitatory interneurons failed to induce lasting functional recovery after SCI. Thus, instead of broadly targeting excitatory or inhibitory neurotransmission, fine-tuning the excitability of inhibitory interneurons appears to be a more effective strategy to make the spinal network receptive to both descending and sensory inputs for successful recovery of motor function.

Translational Perspectives

Based on a selective KCC2 activator identified from high-throughput screening, CLP290 has been optimized for systemic administration (Gagnon et al., 2013) and has been shown to

Figure 5. Altered Neuronal Activation Patterns and Relay Formation Facilitated by CLP290/KCC2

(A) Schematics of transverse spinal cord sections showing c-Fos expression patterns in T8/9 segments after 1 hr of continuous locomotion in intact mice and injured mice with treatment of vehicle, CLP290, AAV-PHP.B-syn-HA-KCC2, or L838,417. Each spot represents a cell positively stained with both c-Fos and NeuN. Representative raw images are shown in Figure S5A.

(B) Average number of c-Fos$^+$ neurons per section in the dorsal zone or the intermediate and ventral zones in all groups. One-way ANOVA, followed by Bonferroni post hoc test (c-Fos$^+$ NeuN$^+$ numbers of the dorsal or intermediate and ventral zones in the vehicle, CLP290-treated, AAV-PHP.B-syn-HA-KCC2-treated, or L838,417-treated groups were compared to that of the intact group, respectively). n = 3 sections per mouse; n = 3 mice per group. *$p < 0.05$; ***$p < 0.001$; ****$p < 0.0001$; ns, not significant. Error bars, SEM.

(C) Average percentage of c-Fos$^+$ neurons per section in laminae 1–5 (dorsal) or in laminae 6–10 (inter-ventral) in all groups. One-way ANOVA, followed by Bonferroni post hoc test (c-Fos$^+$ NeuN$^+$ percentages of the dorsal or intermediate and ventral zones in the vehicle, CLP290-treated, AAV-PHP.B-syn-HA-KCC2-treated, or L838,417-treated groups were compared to that of the intact group, respectively). n = 3 sections per mouse; n = 3 mice per group; *$p < 0.05$; **$p < 0.01$; ***$p < 0.001$; ns, not significant. Error bars, SEM.

(D) Left: schematic of cortical stimulation and TA muscle EMG experiments. Right: representative responses in the right TA muscle evoked by a train of epidural motor cortex stimulations in STA control, AAV-PHP.B-syn-HA-KCC2-treated, CLP290-treated, full transection, and intact groups.

(E) TA muscle EMG response amplitude from indicated groups. One-way ANOVA, followed by Bonferroni post hoc test. n = 3 attempts per mouse; n = 3 mice per group; ***$p < 0.001$; ns, not significant; error bars, SEM.

(F) TA muscle EMG response latency from indicated groups. One-way ANOVA followed by Bonferroni post hoc test. n = 3 attempts per mouse; n = 3 mice per group; ***$p < 0.001$; ns, not significant. Error bars, SEM.

See also Figure S5.

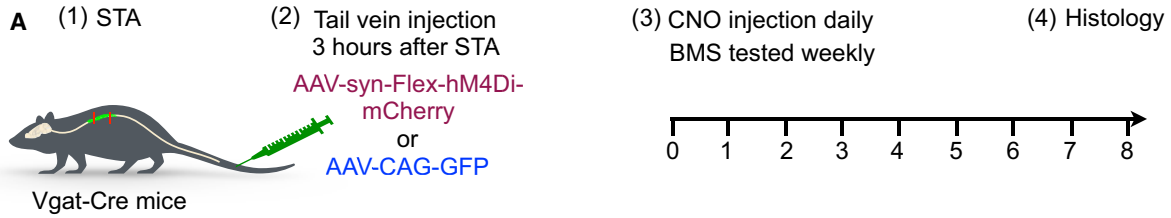

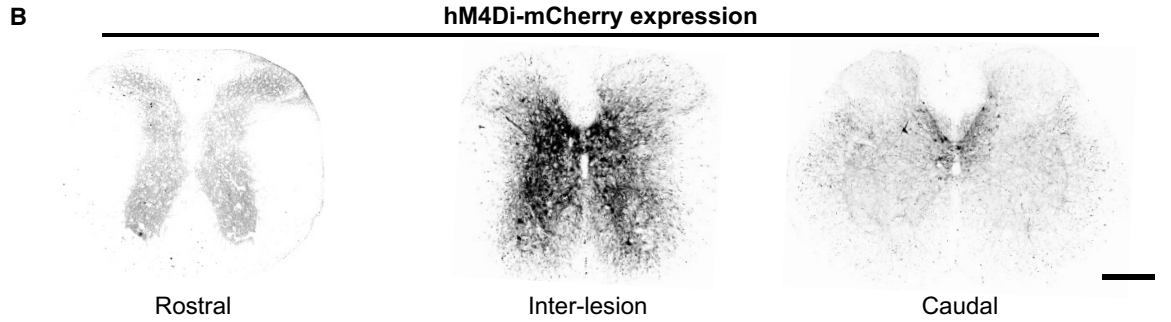

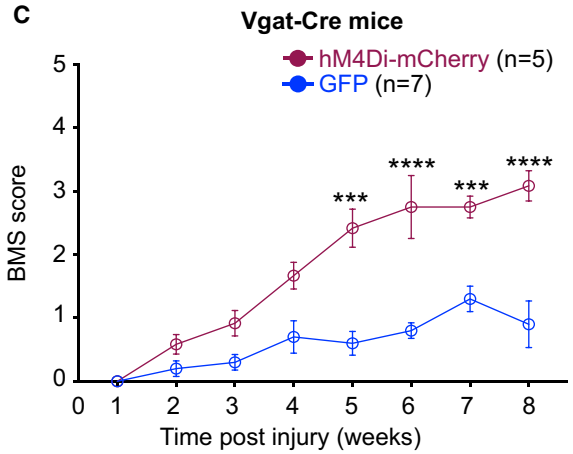

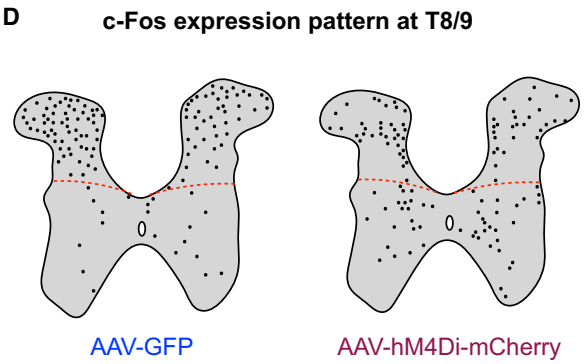

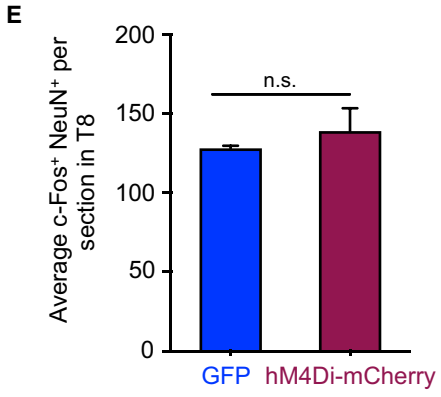

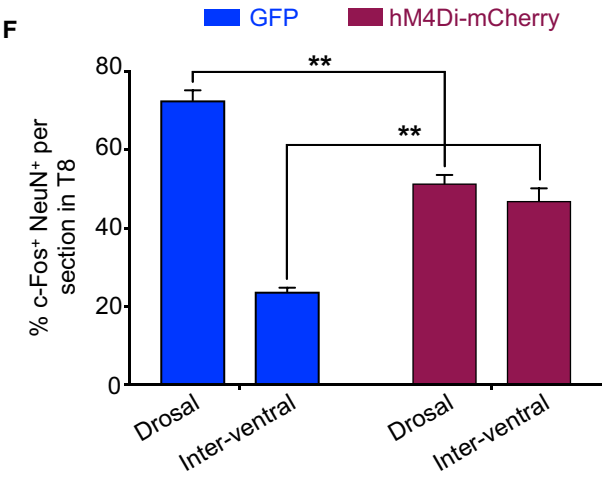

(legend on next page)

effectively treat neuropathic pain in animal models (Ferrini et al., 2017; Gagnon et al., 2013). Unlike other compounds tested in this study, CLP290 exhibited negligible side effects even at high doses (data not shown). Because the majority of SCI patients have some spared axons, our results suggest that the BBB-permeable small molecule CLP290 could be a promising treatment in these cases. Despite this, not all aspects of hindlimb function were restored in these experiments. Thus, future studies should investigate the therapeutic effects of combining CLP290 with other treatments, such as additional rehabilitative training, on hindlimb recovery after SCI.

STAR★METHODS

Detailed methods are provided in the online version of this paper and include the following:

- KEY RESOURCES TABLE
- CONTACT FOR REAGENT AND RESOURCE SHARING
- EXPERIMENTAL MODEL AND SUBJECT DETAILS
  - Mouse Strains
- METHOD DETAILS
  - Chemicals and Antibodies
  - Surgical Procedures
  - Post-surgical treatments and care of the animals
  - Compounds treatment for SCI mice
  - Virus Production and Injection for KCC2 overexpression
  - Anterograde and retrograde tracing experiments
  - Behavioral Experiments
  - EMG Recording and cortical stimulation
  - Immunohistochemistry and Imaging
  - Western Blotting
- QUANTIFICATION AND STATISTICAL ANALYSIS

SUPPLEMENTAL INFORMATION

Supplemental Information includes six figures and one video and can be found with this article online at https://doi.org/10.1016/j.cell.2018.06.005.

ACKNOWLEDGMENTS

We thank Drs. J. Sanes, K. Wang, and C. Woolf for critically reading the manuscript. This study was supported by grants from the National Major Project of Research and Development (2017YFA0104701 to Y.B. and G.X.), NINDS (R01NS096294 to Z.H.), the Craig Neilsen Foundation (384775 to Y. Li and 296466 to Y. Liu), the Paralyzed Veterans of America Research Foundation (PVA_R_0059 to Y. Liu), and the Dr. Miriam and Sheldon G. Adelson Medical Research Foundation (to Z.H.). IDDRC and viral cores were supported by the grants from the NIH (P30 HD018655 and P30EY012196) were used for this study.

AUTHOR CONTRIBUTIONS

B.C. and Z.H. conceived of the project. B.C., Y. Li., B.Y., Z.Z., B.B., Y. Liu., S.Z., J.Z., H.G., Y. Lu, Y.Z., X.G., and Z.H. performed the experiments and discussed the results. P.R.W. and S.V.H. participated in data analysis, and B.C. and Z.H. prepared the manuscript with input from all authors.

DECLARATION OF INTERESTS

The authors declare no competing interests.

Received: November 29, 2017
Revised: March 24, 2018
Accepted: May 31, 2018
Published: July 19, 2018; corrected online: August 30, 2018

REFERENCES

Angeli, C.A., Edgerton, V.R., Gerasimenko, Y.P., and Harkema, S.J. (2014). Altering spinal cord excitability enables voluntary movements after chronic complete paralysis in humans. Brain *137*, 1394–1409.

Arvanian, V.L., Schnell, L., Lou, L., Golshani, R., Hunanyan, A., Ghosh, A., Pearse, D.D., Robinson, J.K., Schwab, M.E., Fawcett, J.W., and Mendell, L.M. (2009). Chronic spinal hemisection in rats induces a progressive decline in transmission in uninjured fibers to motoneurons. Exp. Neurol. *216*, 471–480.

Ballermann, M., and Fouad, K. (2006). Spontaneous locomotor recovery in spinal cord injured rats is accompanied by anatomical plasticity of reticulospinal fibers. Eur. J. Neurosci. *23*, 1988–1996.

Bareyre, F.M., Kerschensteiner, M., Raineteau, O., Mettenleiter, T.C., Weinmann, O., and Schwab, M.E. (2004). The injured spinal cord spontaneously forms a new intraspinal circuit in adult rats. Nat. Neurosci. *7*, 269–277.

Basso, D.M., Fisher, L.C., Anderson, A.J., Jakeman, L.B., McTigue, D.M., and Popovich, P.G. (2006). Basso Mouse Scale for locomotion detects differences in recovery after spinal cord injury in five common mouse strains. J. Neurotrauma *23*, 635–659.

Ben-Ari, Y., Woodin, M.A., Sernagor, E., Cancedda, L., Vinay, L., Rivera, C., Legendre, P., Luhmann, H.J., Bordey, A., Wenner, P., et al. (2012). Refuting the challenges of the developmental shift of polarity of GABA actions: GABA more exciting than ever!. Front. Cell. Neurosci. *6*, 35.

Boulenguez, P., Liabeuf, S., Bos, R., Bras, H., Jean-Xavier, C., Brocard, C., Stil, A., Darbon, P., Cattaert, D., Delpire, E., et al. (2010). Down-regulation of the potassium-chloride cotransporter KCC2 contributes to spasticity after spinal cord injury. Nat. Med. *16*, 302–307.

Figure 6. Gi-DREADD Expression in Inhibitory Interneurons between and around Lesions Mimics the Effects of KCC2/CLP290

(A) Experimental scheme.

(B) Representative images of transverse sections of the thoracic and lumbar spinal cord at 8 weeks post-SCI immunostained with anti-RFP to indicate hM4Di DREADD expression. Scale bar, 100 μm.

(C) BMS performance over time after SCI and virus injections in Gi-DREADD and GFP groups in Vgat-Cre mice. ANOVA followed by post hoc Bonferroni correction. $^{**}p < 0.001$; $^{****}p < 0.0001$; error bars, SEM.

(D). Schematic of transverse spinal cord sections showing c-Fos positive neurons in T8/9 segments after 1 hr of continuous locomotion in AAV-9-Syn-Gi-DREADD-treated mice (dorsal/plantar stepping) and AAV-9-Syn-GFP mice group (dragging).

(E) Average numbers of c-Fos$^+$ neurons (all laminae) per section in indicated groups. Student's t test (two-tailed, unpaired). n = 3 sections per mouse; n = 3 mice per group; ns, not significant. Error bars, SEM.

(F) Percentage of c-Fos$^+$ neurons in laminae 1–5 or laminae 6–10 in indicated groups. Student's t test (two-tailed, unpaired). n = 9 sample slides per group; n = 3 mice per group. $^{**}p < 0.01$; ns, not significant. Error bars, SEM.

See also Figure S6.

Capogrosso, M., Wenger, N., Raspopovic, S., Musienko, P., Beauparlant, J., Bassi Luciani, L., Courtine, G., and Micera, S. (2013). A computational model for epidural electrical stimulation of spinal sensorimotor circuits. J. Neurosci. *33*, 19326–19340.

Cazalets, J.R., Sqalli-Houssaini, Y., and Clarac, F. (1992). Activation of the central pattern generators for locomotion by serotonin and excitatory amino acids in neonatal rat. J. Physiol. *455*, 187–204.

Côté, M.P., Gandhi, S., Zambrotta, M., and Houlé, J.D. (2014). Exercise modulates chloride homeostasis after spinal cord injury. J. Neurosci. *34*, 8976–8987.

Courtine, G., Song, B., Roy, R.R., Zhong, H., Herrmann, J.E., Ao, Y., Qi, J., Edgerton, V.R., and Sofroniew, M.V. (2008). Recovery of supraspinal control of stepping via indirect propriospinal relay connections after spinal cord injury. Nat. Med. *14*, 69–74.

Courtine, G., Gerasimenko, Y., van den Brand, R., Yew, A., Musienko, P., Zhong, H., Song, B., Ao, Y., Ichiyama, R.M., Lavrov, I., et al. (2009). Transformation of nonfunctional spinal circuits into functional states after the loss of brain input. Nat. Neurosci. *12*, 1333–1342.

Cowley, K.C., and Schmidt, B.J. (1995). Effects of inhibitory amino acid antagonists on reciprocal inhibitory interactions during rhythmic motor activity in the in vitro neonatal rat spinal cord. J. Neurophysiol. *74*, 1109–1117.

de Leon, R.D., Tamaki, H., Hodgson, J.A., Roy, R.R., and Edgerton, V.R. (1999). Hindlimb locomotor and postural training modulates glycinergic inhibition in the spinal cord of the adult spinal cat. J. Neurophysiol. *82*, 359–369.

Deverman, B.E., Pravdo, P.L., Simpson, B.P., Kumar, S.R., Chan, K.Y., Banerjee, A., Wu, W.L., Yang, B., Huber, N., Pasca, S.P., and Gradinaru, V. (2016). Cre-dependent selection yields AAV variants for widespread gene transfer to the adult brain. Nat. Biotechnol. *34*, 204–209.

Edgerton, V.R., Courtine, G., Gerasimenko, Y.P., Lavrov, I., Ichiyama, R.M., Fong, A.J., Cai, L.L., Otoshi, C.K., Tillakaratne, N.J., Burdick, J.W., and Roy, R.R. (2008). Training locomotor networks. Brain Res. Brain Res. Rev. *57*, 241–254.

Esposito, M.S., Capelli, P., and Arber, S. (2014). Brainstem nucleus MdV mediates skilled forelimb motor tasks. Nature *508*, 351–356.

Fawcett, J.W., Curt, A., Steeves, J.D., Coleman, W.P., Tuszynski, M.H., Lammertse, D., Bartlett, P.F., Blight, A.R., Dietz, V., Ditunno, J., et al. (2007). Guidelines for the conduct of clinical trials for spinal cord injury as developed by the ICCP panel: spontaneous recovery after spinal cord injury and statistical power needed for therapeutic clinical trials. Spinal Cord *45*, 190–205.

Ferrini, F., Lorenzo, L.E., Godin, A.G., Quang, M.L., and De Koninck, Y. (2017). Enhancing KCC2 function counteracts morphine-induced hyperalgesia. Sci. Rep. *7*, 3870.

Filous, A.R., and Schwab, J.M. (2018). Determinants of axon growth, plasticity, and regeneration in the context of spinal cord injury. Am. J. Pathol. *188*, 53–62.

Frigon, A., and Rossignol, S. (2008). Adaptive changes of the locomotor pattern and cutaneous reflexes during locomotion studied in the same cats before and after spinalization. J. Physiol. *586*, 2927–2945.

Gagnon, M., Bergeron, M.J., Lavertu, G., Castonguay, A., Tripathy, S., Bonin, R.P., Perez-Sanchez, J., Boudreau, D., Wang, B., Dumas, L., et al. (2013). Chloride extrusion enhancers as novel therapeutics for neurological diseases. Nat. Med. *19*, 1524–1528.

Gerasimenko, Y., Roy, R.R., and Edgerton, V.R. (2008). Epidural stimulation: comparison of the spinal circuits that generate and control locomotion in rats, cats and humans. Exp. Neurol. *209*, 417–425.

Grillner, S., and Wallén, P. (1985). Central pattern generators for locomotion, with special reference to vertebrates. Annu. Rev. Neurosci. *8*, 233–261.

Guettier, J.M., Gautam, D., Scarselli, M., Ruiz de Azua, I., Li, J.H., Rosemond, E., Ma, X., Gonzalez, F.J., Armbruster, B.N., Lu, H., et al. (2009). A chemical-genetic approach to study G protein regulation of beta cell function in vivo. Proc. Natl. Acad. Sci. USA *106*, 19197–19202.

Harkema, S., Gerasimenko, Y., Hodes, J., Burdick, J., Angeli, C., Chen, Y., Ferreira, C., Willhite, A., Rejc, E., Grossman, R.G., and Edgerton, V.R. (2011). Effect of epidural stimulation of the lumbosacral spinal cord on voluntary movement, standing, and assisted stepping after motor complete paraplegia: a case study. Lancet *377*, 1938–1947.

He, Z., and Jin, Y. (2016). Intrinsic control of axon regeneration. Neuron *90*, 437–451.

Hofstoetter, U.S., Danner, S.M., Freundl, B., Binder, H., Mayr, W., Rattay, F., and Minassian, K. (2015). Periodic modulation of repetitively elicited monosynaptic reflexes of the human lumbosacral spinal cord. J. Neurophysiol. *114*, 400–410.

Jankowska, E., and Edgley, S.A. (2006). How can corticospinal tract neurons contribute to ipsilateral movements? A question with implications for recovery of motor functions. Neuroscientist *12*, 67–79.

Kaila, K., Ruusuvuori, E., Seja, P., Voipio, J., and Puskarjov, M. (2014). GABA actions and ionic plasticity in epilepsy. Curr. Opin. Neurobiol. *26*, 34–41.

Kakulas, B.A. (1999). A review of the neuropathology of human spinal cord injury with emphasis on special features. J. Spinal Cord Med. *22*, 119–124.

Kato, S., Kobayashi, K., Inoue, K., Kuramochi, M., Okada, T., Yaginuma, H., Morimoto, K., Shimada, T., Takada, M., and Kobayashi, K. (2011). A lentiviral strategy for highly efficient retrograde gene transfer by pseudotyping with fusion envelope glycoprotein. Hum. Gene Ther. *22*, 197–206.

Kiehn, O. (2006). Locomotor circuits in the mammalian spinal cord. Annu. Rev. Neurosci. *29*, 279–306.

Kiehn, O. (2016). Decoding the organization of spinal circuits that control locomotion. Nat. Rev. Neurosci. *17*, 224–238.

Kinoshita, M., Matsui, R., Kato, S., Hasegawa, T., Kasahara, H., Isa, K., Watakabe, A., Yamamori, T., Nishimura, Y., Alstermark, B., et al. (2012). Genetic dissection of the circuit for hand dexterity in primates. Nature *487*, 235–238.

Knabl, J., Witschi, R., Hösl, K., Reinold, H., Zeilhofer, U.B., Ahmadi, S., Brockhaus, J., Sergejeva, M., Hess, A., Brune, K., et al. (2008). Reversal of pathological pain through specific spinal GABAA receptor subtypes. Nature *451*, 330–334.

Krashes, M.J., Koda, S., Ye, C., Rogan, S.C., Adams, A.C., Cusher, D.S., Maratos-Flier, E., Roth, B.L., and Lowell, B.B. (2011). Rapid, reversible activation of AgRP neurons drives feeding behavior in mice. J. Clin. Invest. *121*, 1424–1428.

Liu, K., Lu, Y., Lee, J.K., Samara, R., Willenberg, R., Sears-Kraxberger, I., Tedeschi, A., Park, K.K., Jin, D., Cai, B., et al. (2010). PTEN deletion enhances the regenerative ability of adult corticospinal neurons. Nat. Neurosci. *13*, 1075–1081.

Liu, Y., Wang, X., Li, W., Zhang, Q., Li, Y., Zhang, Z., Zhu, J., Chen, B., Williams, P.R., Zhang, Y., et al. (2017). A sensitized IGF1 treatment restores corticospinal axon-dependent functions. Neuron *95*, 817–833.e4.

Möhler, H., Fritschy, J.M., Crestani, F., Hensch, T., and Rudolph, U. (2004). Specific GABA(A) circuits in brain development and therapy. Biochem. Pharmacol. *68*, 1685–1690.

O'Shea, T.M., Burda, J.E., and Sofroniew, M.V. (2017). Cell biology of spinal cord injury and repair. J. Clin. Invest. *127*, 3259–3270.

Pearson, K.G., Acharya, H., and Fouad, K. (2005). A new electrode configuration for recording electromyographic activity in behaving mice. J. Neurosci. Methods *148*, 36–42.

Robinson, G.A., and Goldberger, M.E. (1986). The development and recovery of motor function in spinal cats. II. Pharmacological enhancement of recovery. Exp. Brain Res. *62*, 387–400.

Rosenzweig, E.S., Courtine, G., Jindrich, D.L., Brock, J.H., Ferguson, A.R., Strand, S.C., Nout, Y.S., Roy, R.R., Miller, D.M., Beattie, M.S., et al. (2010). Extensive spontaneous plasticity of corticospinal projections after primate spinal cord injury. Nat. Neurosci. *13*, 1505–1510.

Rossi, J., Balthasar, N., Olson, D., Scott, M., Berglund, E., Lee, C.E., Choi, M.J., Lauzon, D., Lowell, B.B., and Elmquist, J.K. (2011). Melanocortin-4 receptors expressed by cholinergic neurons regulate energy balance and glucose homeostasis. Cell Metab. *13*, 195–204.

Rossignol, S., and Barbeau, H. (1993). Pharmacology of locomotion: an account of studies in spinal cats and spinal cord injured subjects. J. Am. Paraplegia Soc. *16*, 190–196.

Rossignol, S., and Frigon, A. (2011). Recovery of locomotion after spinal cord injury: some facts and mechanisms. Annu. Rev. Neurosci. *34*, 413–440.

Roth, B.L. (2016). DREADDs for Neuroscientists. Neuron *89*, 683–694.

Sawada, M., Kato, K., Kunieda, T., Mikuni, N., Miyamoto, S., Onoe, H., Isa, T., and Nishimura, Y. (2015). Function of the nucleus accumbens in motor control during recovery after spinal cord injury. Science *350*, 98–101.

Schucht, P., Raineteau, O., Schwab, M.E., and Fouad, K. (2002). Anatomical correlates of locomotor recovery following dorsal and ventral lesions of the rat spinal cord. Exp. Neurol. *176*, 143–153.

Takeoka, A., Vollenweider, I., Courtine, G., and Arber, S. (2014). Muscle spindle feedback directs locomotor recovery and circuit reorganization after spinal cord injury. Cell *159*, 1626–1639.

Tong, Q., Ye, C., McCrimmon, R.J., Dhillon, H., Choi, B., Kramer, M.D., Yu, J., Yang, Z., Christiansen, L.M., Lee, C.E., et al. (2007). Synaptic glutamate release by ventromedial hypothalamic neurons is part of the neurocircuitry that prevents hypoglycemia. Cell Metab. *5*, 383–393.

van den Brand, R., Heutschi, J., Barraud, Q., DiGiovanna, J., Bartholdi, K., Huerlimann, M., Friedli, L., Vollenweider, I., Moraud, E.M., Duis, S., et al. (2012). Restoring voluntary control of locomotion after paralyzing spinal cord injury. Science *336*, 1182–1185.

Vong, L., Ye, C., Yang, Z., Choi, B., Chua, S., Jr., and Lowell, B.B. (2011). Leptin action on GABAergic neurons prevents obesity and reduces inhibitory tone to POMC neurons. Neuron *71*, 142–154.

Wang, X., Liu, Y., Li, X., Zhang, Z., Yang, H., Zhang, Y., Williams, P.R., Alwahab, N.S.A., Kapur, K., Yu, B., et al. (2017). Deconstruction of corticospinal circuits for goal-directed motor skills. Cell *171*, 440–455.e14.

Wenger, N., Moraud, E.M., Raspopovic, S., Bonizzato, M., DiGiovanna, J., Musienko, P., Morari, M., Micera, S., and Courtine, G. (2014). Closed-loop neuromodulation of spinal sensorimotor circuits controls refined locomotion after complete spinal cord injury. Sci. Transl. Med. *6*, 255ra133.

Zaporozhets, E., Cowley, K.C., and Schmidt, B.J. (2011). Neurochemical excitation of propriospinal neurons facilitates locomotor command signal transmission in the lesioned spinal cord. J. Neurophysiol. *105*, 2818–2829.

Zörner, B., Filli, L., Starkey, M.L., Gonzenbach, R., Kasper, H., Röthlisberger, M., Bolliger, M., and Schwab, M.E. (2010). Profiling locomotor recovery: comprehensive quantification of impairments after CNS damage in rodents. Nat. Methods *7*, 701–708.

STAR★METHODS

KEY RESOURCES TABLE

REAGENT or RESOURCE	SOURCE	IDENTIFIER
Antibodies		
Chicken monoclonal anti-GFP	Abcam	Cat#ab13970
Rabbit polyclonal anti-RFP	Abcam	Cat#ab34771
Mouse monoclonal anti-NeuN	Millipore	Cat#MAB377
Rabbit polyclonal anti-5-HT	Immunostar	Cat#20080
Rat monoclonal anti-HA	Sigma	Cat#11867423001
Rabbit polyclonal anti-GFAP	DAKO	Cat#Z0334
Rabbit polyclonal anti-c-Fos	Cell signaling	Cat#2250s
Rabbit polyclonal anti-KCC2	Milipore	Cat#07-432
Chemicals, Peptides, and Recombinant Proteins		
Quipazine	Sigma	Cat# Q1004
8-OH-DPAT	Tocris	Cat#0529
Clozapine N-oxide	Enzo Life Sciences	Cat#BML-NS105-0025
Baclofen	Tocris	Cat#0417
CP101606	Sigma	Cat#SML0053
CLP290	PharmaBlock	Cat#N/A
L838,417	PharmaBlock	Cat#PBLJ6533
Bumetanide	Tocris	Cat#3108
Experimental Models: Organisms/Strains		
Mouse/ C57BL/6	Charles River	Strain code#027
Mouse/ Vgat-ires-Cre	The Jackson Laboratory	Jax#28862
Mouse/Vglut2-ires-Cre	The Jackson Laboratory	Jax#28863
Mouse/ChAT-ires-Cre	The Jackson Laboratory	Jax#28861
Recombinant DNA		
AAV-syn-mCherry	This paper	N/A
AAV-syn-FLEX-HA-KCC2	This paper	N/A
AAV-syn-FLEX-hM4Di-mCherry	Krashes et al., 2011	Addgene Cat#44362
AAV-syn-FLEX-hM3Dq-mCherry	Krashes et al., 2011	Addgene Cat#44361
AAV-CAG-FLEX-H2B-GFP	Vigenebio	N/A
AAV-CAG-H2B-GFP	This paper	N/A
AAV-CAG-GFP-WPRE	Wang et al., 2017	N/A
AAV-syn-HA-KCC2	This paper	N/A
Lenti-HiRet-mCherry	Liu et al., 2017	N/A
Software and Algorithms		
MATLAB 2017	Mathworks	https://www.mathworks.com/
ImageJ2/Fiji	NIH	https://imagej.nih.gov/ij/
Simi Motion	SIMI reality motion systems	https://www.simi.com/en/
STATA version 12	STATA software	https://www.stata.com/
Prism version 7.0 for Mac	GraphPad Software, Inc	https://www.graphpad.com/scientific-software/prism/

CONTACT FOR REAGENT AND RESOURCE SHARING

Further information and requests for resources and reagents should be directed to and will be fulfilled by the Lead Contact, Zhigang He (zhigang.he@childrens.harvard.edu).

EXPERIMENTAL MODEL AND SUBJECT DETAILS

Mouse Strains

All experimental procedures were performed in compliance with animal protocols approved by the Institutional Animal Care and Use Committee at Boston Children's Hospital. Mice employed in this study included: C57BL/6 wild-type (WT) mouse (Charles River, Strain code#027); Vgat-ires-Cre (Jax#28862), VGlut2-ires-Cre (Jax#28863) and ChAT-ires-Cre (Jax#28861) mouse strains maintained on C57BL/6 genetic background. For behavioral measurements, all experimental animals used were from different littermates. 19∼21 g adult female mice at the age of 8 weeks were randomized and assigned to different treatment groups, prior to injury, and no other specific randomization was used for the animal studies.

METHOD DETAILS

Chemicals and Antibodies

For systemic administration (i.p.): Quipazine [Sigma (Q1004), 0.2 mg/kg)] and 8-OH-DPAT [Tocris (0529), 0.1 mg/kg)] were suspended in 0.9% NaCl; Baclofen [Tocris (0417), 1 mg/kg)] was suspended in 100mM NaOH and then 0.9% NaCl; CP101606 [Sigma (SML0053), 10 mg/kg)] was suspended in DMSO and then 0.9% NaCl; CLP290 [synthesized by PharmaBlock, 35mg/kg] was suspended in DMSO and then 20% 2-hydroxypropyl- β-cyclodextrin; L838,417 [synthesized by PharmaBlock, 1mg/kg] was suspended in 0.5% methylcellulose and 0.9% NaCl; and Bumetanide [Tocris, (3108), 0.3 mg/kg)] was suspended in 15% DMSO. For immunostaining and western blotting, the primary antibodies used were: chicken anti-GFP [Abcam (Cat: ab13970)], rabbit anti-RFP [Abcam (Cat: ab34771)], rabbit anti-GFAP [DAKO (Z0334)], rabbit anti-5-HT [Immunostar (20080)], rat anti-HA [Sigma (11867423001)], rabbit anti-c-Fos [Cell signaling (2250s)], mouse anti-NeuN [Millipore (MAB377)]; and rabbit anti-KCC2 [Milipore (07-432)].

Surgical Procedures

The procedure of T7 and T10 double lateral hemisection was similar to that described elsewhere (Courtine et al., 2008; van den Brand et al., 2012). Briefly, a midline incision was made over the thoracic vertebrae, followed by a T7-10 laminectomy. For the T7 right side over-hemisection, we carefully used both a scalpel and micro-scissors to interrupt the bilateral dorsal column at T7, and ensured no sparing of ventral pathways on the contralateral side (Figure 1A). For the T10 left hemisection, we carefully used both a scalpel and micro-scissors to interrupt only the left side of the spinal cord until the midline. The muscle layers were then sutured, and the skin was secured with wound clips. All animals received post hoc histological analysis, and those with spared 5HT axons at the lumbar spinal cord (L2-5) were excluded for behavioral analysis (Figure S1).

The procedure of T8 full transection was similar to that described elsewhere (Courtine et al., 2009). Briefly, a midline incision was made over the thoracic vertebrae, followed by a T8 laminectomy. The complete T8 transection was then performed carefully using both a scalpel and micro-scissors. The muscle layers were then sutured and the skin was secured with wound clips. All surgeries were completed by a surgical technician, who was blind to the experimental conditions.

Post-surgical treatments and care of the animals

After SCI in adult mice, we injected subcutaneously 1ml of saline, placed some food on the cage floor and kept the mice warm until awakening. Twice a day, we manually emptied their bladders, checked hydration and monitored any clinical signs of pain or infection. We treated any urinary infection with an antibiotherapy (Baytril, 10mg/kg, for 5 days). We sacrificed mice presenting a more than 15% decrease in body weight.

Compounds treatment for SCI mice

Prior to double latereal hemisection, adult female WT mice at the age of 8 weeks were randomized and assigned to 8 different groups (n = 10 for each group). 1 week post SCI, Quipazine, 8-OH-DPAT, Baclofen, CP101606, CLP290, L838,417, Bumetanide and saline were delivered via intraperitoneal injection (Dissolve conditions and concentration listed in the Chemical and Antibodies section) to each mouse in individual groups daily until the mice were sacrificed. For CLP290 treatment experiments, we carried out 2 additional replications, adult 8 weeks female mice were randomized and assigned to 2 different groups: 20% 2-hydroxypropyl-β-cyclodextrin (vehicle solution) and CLP290. In both groups, animal number started as n = 10. CLP290 and vehicle solution also delivered into T8 full transection mice, the compounds delivery methods were the same as the treatment for double lateral hemisection mice. In both groups, animal number started as n = 10.

After post-mortem histological analysis, mice with spared 5HT axons observed at lumbar spinal cord level, i.e., incomplete hemisections were excluded: 20% 2-hydroxypropyl-β-cyclodextrin (vehicle solution) group (n = 1), bumetanide group (n = 2), L838,417 group (n = 1), 8-OH-DPAT group (n = 1) and quipazine group (n = 1) respectively.

Virus Production and Injection for KCC2 overexpression

All viruses used in this paper were produced by the Viral Core, Boston Children's Hospital. For the KCC2 overexpression virus injection procedure, AAV2/PHP.B-Syn-HA-KCC2 and AAV2/9-Syn-HA-KCC2 were injected into the tail vein of WT mice. AAV2/PHP.B-Syn-FLEX-HA-KCC2 was injected to Vgat-Cre, Vglut2-Cre and ChAT-Cre mice tail vein. AAV2/9-Syn-HA-KCC2 and AAV2/9-Syn-FLEX-HA-KCC2, AAV2/9-Syn-FLEX-hM4Di-mCherry and AV2/9-Syn-FLEX-hM3Dq-mCherry, were injected into WT, Vgat-Cre or Vglut2-cre mice tail vein. Tail vein virus injection was performed, as described previously (Deverman et al., 2016), 3 hours after SCI (AAV titers were adjusted to 4-5x10^{13} copies/ml for injection). Briefly, the mouse tail was swabbed with alcohol then injected intravenously with a 200 ul viral solution containing a mixture of sterile PBS with a 30G needle.

AAV2/1-Syn-HA-KCC2 and AAV2/1-Syn-FLEX-HA-KCC2 were intraspinally injected into the lumbar level (L2-4) of WT and Vgat-Cre mice, respectively. Lumbar level intraspinal virus injection was performed one day prior to SCI procedure, in order to eliminate any possible behavioral defects caused by lumbar level intraspinal injection (AAV titers were adjusted to 0.5-1x10^{13} copies/ml for injection). After post-mortem histological analysis of all mice with virus treatment, 1 mouse from AAV2/PHP.B-Syn-FLEX-HA-KCC2 + ChAT-Cre mice was excluded due to spared 5HT axons observed in the lumbar spinal cord level. For AAV2/PHP.B-Syn-HA-KCC2 and AAV2/9-Syn-HA-KCC2 injections to WT mice experiments, we carried out 2 additional replications for all groups, animal number started as n = 10.

Anterograde and retrograde tracing experiments

For reticulospinal anterograde tracing experiments (procedure was described previously) (Esposito et al., 2014), AAV2/8-ChR2-YFP and AAV2/8-ChR2-mCherry were injected into the mouse right and left reticular formation in the brain stem respectively. Injection coordinates were –1.5, −2.0, −2.5mm caudal, ± 0.4mm lateral to lambda, and −4.5mm verntral from the surface of cerebellum (6 injections per side, 100nl per injection). For CST tracing experiments (procedure was described previously) (Liu et al., 2010, 2017), AAV2/8-ChR2-mCherry was injected to the mouse right sensorimotor cortex (all AAV titers were adjusted to 0.5-5x10^{13} copies/ml for injection). Injection coordinates were 1, 0.5, 0, −0.5, −1, and −1.5mm caudal, 1.3mm lateral to bregma, and 0.6mm ventral from the surface of the brain (6 injection in right side, 100nl per injection).

For lumbar level retrograde tracing, vectors of HiRet-mCherry (lenti-virus titers were adjusted to 1.6-2x10^{12} copies/ml for injection) were constructed based on the HiRet-lenti backbone (Kinoshita et al., 2012). Injection procedure was described previously (Wang et al., 2017), in which HiRet-mCherry is injected into left or right lumbar spinal cord from segments 2-4. Injection coordinates were 0.5mm lateral of the midline, and 3 injection sites were separated 1mm away, in each injection site, 3 injections were performed at 3 different depths, 0.4mm, 0.8mm and 1.2mm (9 injections per side, 100nl per injection).

Behavioral Experiments

Motor function was evaluated weekly with a locomotor open field rating scale, the Basso Mouse Scale (BMS). All BMS behavior tests were examined by investigators blinded to the treatment groups. For transient pharmacological treatments, ten to fifteen minutes (van den Brand et al., 2012) prior to behavioral tests (grounding walking, all of which were performed individually), mice received systematic administration (i.p.) of the neural modulators listed above or CNO. It is important to note that with a single intraperitoneal injection, plasma CNO levels peak at 15 min and become very low by 2 h after injection (Guettier et al., 2009). For chronic pharmacological treatments, 24 hours prior to behavioral tests, mice received systematic administration of the compounds listed above. All behavioral tests were completed within 1-3 hours.

For detailed hindlimb kinematic analysis, mice from different groups were placed in the MotoRater (TSE Systems) (Zörner et al., 2010), and all kinematic analysis was performed based on data collected by the MotoRater. Briefly, mice from different treatment groups (CLP290, vehicle control, AAV-KCC2 and AAV-GFP) were placed in a clear Plexiglas runway, 123 cm long, 4 cm wide and 15 cm high to assess over ground locomotion (vehicle control n = 8, other groups n = 10). Anatomical landmarks on the hindlimb were highlighted at the iliac crest, hip joint, knee joint, ankle and toe. For each mouse in each group, 6-10 continuous gait cycles were captured using the TSE high-speed capture system (TSE Systems, Germany, https://www.tse-systems.com/), and videos were analyzed offline by Simi motion software (Simi reality motion system, Germany). Bony land markers were used to measure iliac crest height, stride length, knee and ankle angle oscillation for each gait cycle for different treatment groups. The kinematic data were analyzed blindly by an investigator, and stick view of hindlimb movement were drawn using MATLAB blindly by a technician.

EMG Recording and cortical stimulation

The procedure for EMG recording in free moving animals was similar to that described previously (Pearson et al., 2005). In brief, at 9 weeks after surgery, 5 mice were randomly chosen from each group (Control, CLP290 and AAV-KCC2 treated mice) underwent implantation of customized bipolar electrodes into selected hindlimb muscles to record EMG activity. Electrodes (793200, A-M Systems) were led by 30 gauge needles and inserted into the mid-belly of the medial gastrocnemius (GS) and tibialis anterior (TA) muscles of the right hindlimb. A common ground wire was inserted subcutaneously in the neck-shoulder area. Wires were routed subcutaneously through the back to a small percutaneous connector securely cemented to the skull of the mouse. EMG signals were acquired using a differential AC amplifier (1700, A-M Systems, WA) with 10-1000 Hz filtration, sampled at 4 kHz using a digitizer (PowerLab 16/35, ADInstruments), and analyzed by LabChart 8 (ADInstruments) by an ivestigators blinded to experimental groups.

For epidural stimulation and EMG recording, a customized head plate was secured over the skull, and a monopolar stimulation electrode (SSM33A05, World Precision Instruments) was positioned epidurally over the representative hindlimb area of left motor cortex. A train of electrical stimuli (0.2ms biphasic pulse, 100ms pulse train, 20 Hz, 0.5-1.5 mA) was generated by pulse generator and isolator (Master 9 and Iso-Flex, A.M.P.I.), and delivered during quadrupedal standing in fully awake condition. Testing was performed without and with electrochemical stimulations. Peak-to-peak amplitude and latency of evoked responses were computed from EMG recordings of the right TA muscle. EMG recordings were examined by an assessor blinded to the treatment groups.

Immunohistochemistry and Imaging

The paraformaldehyde (PFA) fixed tissues were cryo-protected with 30% sucrose and processed using cryostat (section thickness 40 μm for spinal cord). Sections were treated with a blocking solution containing 10% normal donkey serum with 0.5% Triton-100 for 2 hours at room temperature before staining. The primary antibodies (4°, overnight) used were: rabbit anti-GFAP [DAKO (Z0334), 1:600]; rabbit anti-5-HT [Immunostar (20080), 1: 5,000]; chicken anti-GFP [Abcam (ab13970), 1:400]; rabbit anti-RFP [Abcam (ab34771), 1:400]; rat anti-HA [Sigma (11867423001), 1:200]; rabbit anti-c-Fos [Cell signaling (2250s), 1:100]; and mouse anti-NeuN [Millipore (MAB377), 1:400]. Secondary antibodies (room temperature, 2h) included: Alexa Fluor 488-conjugated donkey anti chicken and rabbit; and Alexa Fluor 594-conjugated donkey anti rabbit (all from Invitrogen). c-Fos immunoreactivity of spinal neurons was determined as previously described (Courtine et al., 2009), after 1-hour of continuous quadrupedal free walking (intact), stepping (CLP290 or AAV-KCC2 treated mice) or dragging (vehicle or AAV-GFP treated mice). The mice were returned to their cages, and were then anesthetized and sacrificed by intracardial perfusion of 4% PFA (wt/vol) in phosphate buffered saline (PBS) about 2 hours later.

Spinal cord transverse and horizontal sections were imaged with a confocal laser-scanning microscope (Zeiss 700 or Zeiss 710). To quantify and compare fluorescence intensity of: reticular spinal tract projections (RFP^+ and GFP^+), and corticospinal tract (CST) projections (GFP^+), at different transverse spinal cord segments sections (Figures S4A and S4C); as well as 5HT axonal staining (Figure S4B). All images, used for analysis under multiple conditions, were taken using the same optical parameters to avoid saturation. Densitometry measurements were taken by using FIJI software, after being sub-thresholded to the background and normalized by area. The images were acquired and analyzed blindly by a separate analyzer.

To quantify and compare the retrograde HiRet-marked cell body of spinal neurons in different treatments, all images were decomposed to individual channels and planes. They were aligned and quantified using custom-developed MATLAB codes. HiRet-marked neurons were assigned coordinates manually. The images were then analyzed blindly by a separate analyzer.

Western Blotting

Animals were killed by decapitation after isoflurane anesthesia. Spinal cords were quickly dissected out from T5 to L1 and divided into 350 μm slices. Samples were homogenized in cold lysis buffer containing: 20 mmol/L Tris (pH 7.4), 125 mmol/L NaCl, 10% glycerol, 1% Triton X-100,0.5% DCA, 0.1% SDS, 20 mmol/L NaF, 1 mmol/L phenylmethylsulfonyl fluoride, 4 μg/mL aprotinin, 4 μg/mL leupeptin, and 1 mmol/L Na3VO4. Then samples were centrifuged at 13,000 g for 10 minutes at 4°C. Protein concentrations in supernatant were assessed using the bicinchoninic acid protein assay kit (Bio-Rad, Hercules, CA). Equal amounts of protein extracts were resolved by 4%–20% SDS-PAGE and electrotransferred onto polyvinylidene difluoride membranes (Millipore, Bedford, MA). After blockade in Tris-buffered saline plus 3% BSA, membranes were exposed to a polyclonal rabbit KCC2-specific antibody diluted 1 in 500 (Millipore), or a polyclonal rabbit beta-actin antibody diluted 1 in 2000 (cell signaling), in the blocking solution overnight at 4°C. ImmunoPure goat horseradish peroxidase–conjugated rabbit-specific antibodies were used (1 in 500 in blocking solution, 1 h at 22°C) for chemiluminescent detection (Pierce Biotech).

QUANTIFICATION AND STATISTICAL ANALYSIS

The normality and variance similarity were measured by STATA (version 12, College station, TX, USA) before we applied any parametric tests. Sample sizes were estimated based on previous SCI studies using similar animal models. Moreover, considering our treatment methods require an approximately 10 weeks, therefore, we decided to start each group with 8-10 mice. Sample sizes (n) of animal numbers of biological repeats of experiments and statistical methods used are indicated in the corresponding figure legends. Two-tailed Student's t test was used for the single comparison between two groups. The rest of the data were analyzed using one-way or two-way ANOVA depending on the appropriate design. *Post hoc* comparisons were carried out only when the primary measure showed statistical significance. P value of multiple comparisons was adjusted by using Bonferroni's correction. Error bars in all figures represent mean ± SEM. Differences were considered statistically significant at p value below 0.05. All data were analyzed using GraphPad Prism version 7.0 software for Mac and STATA version 12.

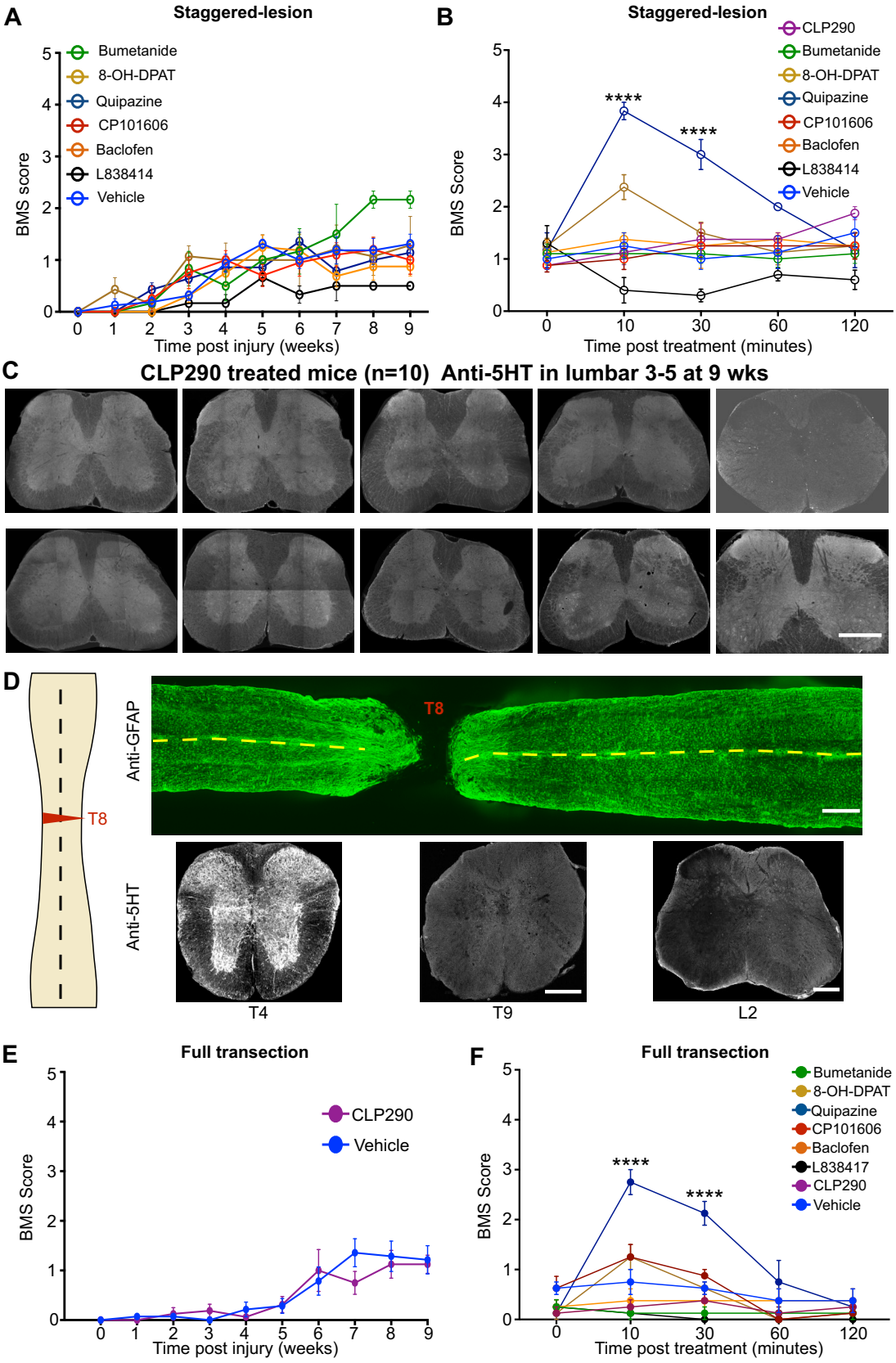

(legend on next page)

Figure S1. The Effects of Small Molecule Compounds in Mice with Staggered or Complete Spinal Cord Injury, Related to Figure 1

(A) BMS scores measured at 24 hr after compound administration in stagger-lesioned mice with continuous treatment of indicated compounds. Repeated-measures ANOVA followed by post hoc Bonferroni correction. All groups started as n = 10, and at week 9 (the termination time point) n = 8, 10, 3, 8, 4, 7 and 7 for saline, CP101606 (10mg/Kg), bumetanide (0.3mg/Kg), baclofen (1mg/Kg), L838,417 (1mg/Kg), 8-OH-DPAT (0.1mg/Kg) and quipazine (0.2mg/Kg) respectively. Error bars, SEM.

(B) BMS scores measured acutely after compound treatments (10, 30, 30, 60 and 120 min after compound administration) in stagger-lesioned mice at 8 weeks after SCI. Two way repeated-measures ANOVA followed by post hoc Bonferroni correction. All groups n = 5, ****$p < 0.0001$; error bars, SEM.

(C) Representative confocal images of transverse sections, stained with anti-5HT antibody, from L2 spinal level of injured mice with CLP290 treatment at 10 weeks post staggered injury. Scale bar: 100 μm.

(D) Left, Schematic of full transection (FT) at T8. Arrowhead indicates lesion. Right top: Representative confocal image stack of a longitudinal spinal cord section (from T5 to T12) at 10 weeks post FT lesion immunostained with anti-GFAP. Dashed line indicates midline. Scale bar: 500 μm. Right bottom: Representative confocal image stacks of transverse sections from the thoracic and lumbar spinal cord (T5, rostral to lesions, T9 and L2, caudal to lesion) at 8 weeks post over-stagger lesion immunostained with anti-5HT (serotonergic axons). Scale bar: 100 μm.

(E) BMS scores measured at 24 hr after vehicle or CLP290 administration in mice with full transection. Repeated-measures ANOVA followed by post hoc Bonferroni correction. Both groups started as n = 10, and at week 9 (the termination time point) n = 8, and 10 for vehicle and CLP290 respectively. Error bars, SEM.

(F) BMS scores measured acutely after compound treatments (10, 30, 30, 60 and 120 min after compound administration) at 8 weeks in mice after full transection without chronic treatments. Repeated-measures ANOVA followed by post hoc Bonferroni correction. All groups n = 5, ****$p < 0.0001$; error bars, SEM.

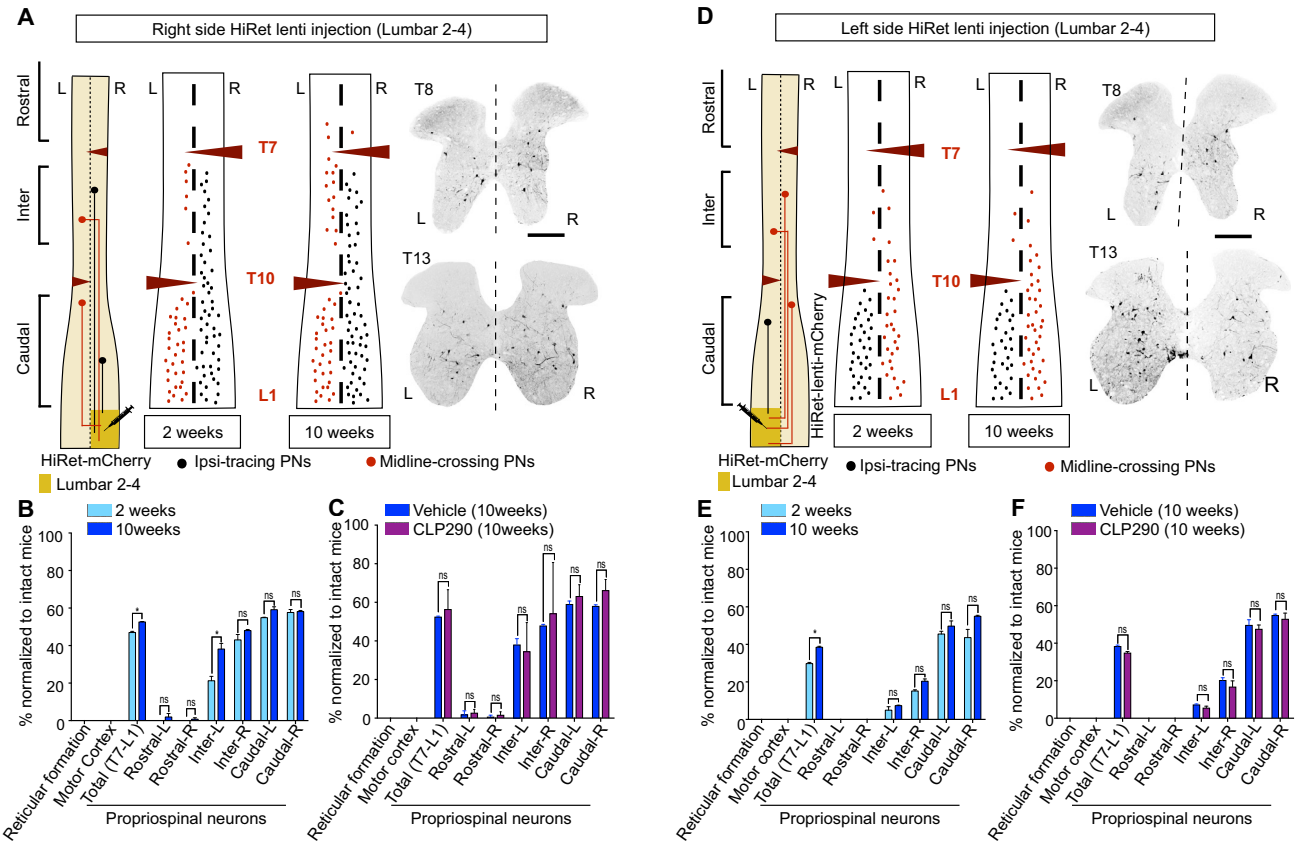

Figure S2. No Significant Effects of CLP290 on Axon Growth (Retrograde Labeling), Related to Figure 1

(A) Left: Schematic of HiRet-mCherry injection to retrogradely labeled propriospinal and brain neurons with descending projections to right side lumbar spinal cord (L2-4). Mice received HiRet-mCherry injection at either 1 day (acute) or 8 weeks (chronic) after injury. The mice were terminated at 2 weeks after viral injection for histological analysis. Middle: Longitudinal representations of propriospinal neurons labeled at acute and chronic stages. Each dot represents 5 neurons. Right: Representative confocal image stacks of transverse sections of T8 (between the lesions) and T13 (below the lesions) at 10 weeks post staggered injury stained with anti-RFP. Scale bar: 100 μm. Bottom: Ipsi-tracing PNs: ipsilateral tracing propriospinal neurons, Midline-crossing PNs: middle line crossing propriospinal neurons (relative to injection site).

(B and C) Quantification of labeled neurons in the brain and spinal cord from A. Numbers of retrogradely labeled neurons in different brain regions and spinal segments in mice with vehicle treatment at acute and chronic stages (B) or in mice with vehicle or CLP290 treatment at chronic stage (C) were normalized to those retrogradely labeled neurons in intact mice Rostral: above T7; inter, T8-T10; caudal: T10-L1. L: left, R: right. Student's t test; n = 3 each for intact, acute and chronic SCI mice. *p < 0.05, n.s. not significant. Error bars: SEM.

(D) Left: Schematic of HiRet-mCherry injection to retrogradely label propriospinal and brain neurons with descending projections to left side lumbar spinal cord (L2-4). Animals received HiRet-mCherry injection at either 1 day (acute) or 8 weeks (chronic) after staggered injury. The mice were terminated at 2 weeks after viral injection for histological analysis. Middle: Longitudinal representations of propriospinal neurons labeled at acute and chronic stages. Each dot represents 5 neurons. Right: Representative confocal image stacks of transverse sections of T8 (between the lesions) and T13 (below the lesions) at 10 weeks post staggered injury stained with anti-RFP. Scale bar: 100 μm. Bottom: Ipsi-tracing PNs: ipsilateral tracing propriospinal neurons, Midline-crossing PNs: middle line crossing propriospinal neurons (relative to injection site).

(E and F) Quantification of labeled neurons in the brain and spinal cord from D. Numbers of mCherry-marked of brain and propriospinal neurons in different spinal segments in mice with vehicle treatment at acute and chronic stages (E) or in mice with vehicle or CLP290 treatment at chronic stage (F) were normalized to those retrogradely labeled neurons in intact mice. Rostral: above T7; inter, T8-T10; caudal: T10-L1. L: left, R: right. Student's t test; n = 3 each for intact, acute and chronic SCI mice. *p < 0.05, n.s. not significant. Error bars: SEM.

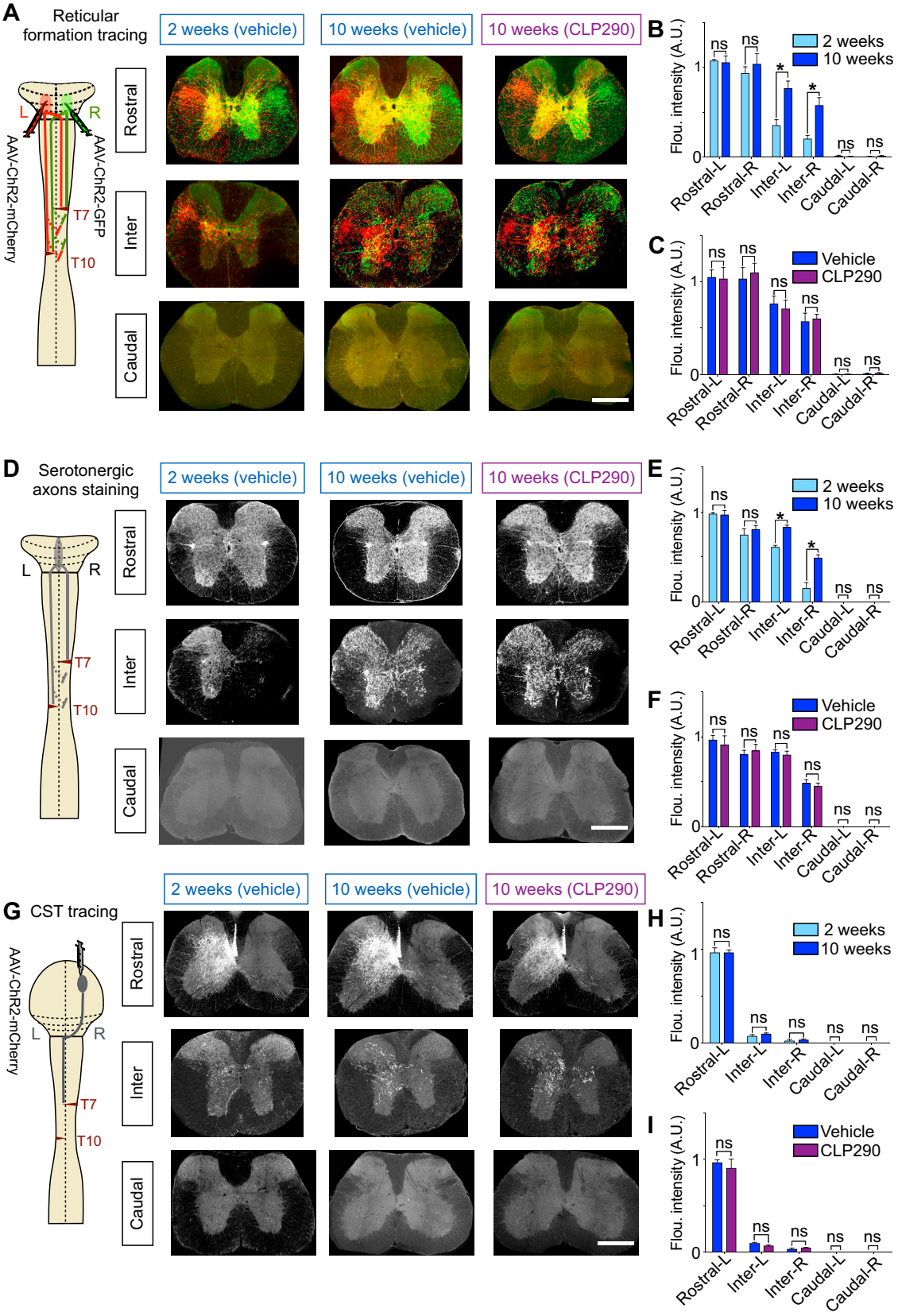
A
Reticular formation tracing
2 weeks (vehicle)
10 weeks (vehicle)
10 weeks (CLP290)
Rostral
Inter
Caudal
L
R
AAV-ChR2-mCherry
AAV-ChR2-GFP
T7
T10
B
Flou. intensity (A.U.)
2 weeks
10 weeks
ns
*
Rostral-L
Rostral-R
Inter-L
Inter-R
Caudal-L
Caudal-R
C
Vehicle
CLP290
D
Serotonergic axons staining
E
F
G
CST tracing
H
I
(legend on next page)

Figure S3. No Effects of CLP290 on Axon Growth of Descending Axons, Related to Figure 1

(A) Left: Schematic of AAV injection strategy for anterograde labeling of neurons from brainstem reticular formation. Animals received an injection of AAV-ChR2-mCherry (left) and AAV-ChR2-GFP (right side) at either 1 day (acute) or 8 weeks (chronic) after injury. The mice were terminated at 2 weeks after viral injection for histological analysis. Red line: axons descending from left side reticular formation; green line: axons descending from right side reticular formation. Right: Representative confocal image stacks of transverse sections of the thoracic and lumbar spinal cord at 2 weeks and 10 weeks post injury stained with anti-RFP (red) and anti-GFP (green). Scale bar: 100 μm.

(B) The fluorescence intensity of mCherry and GFP immunostaining at 2 weeks and 10 weeks post staggered injury in vehicle treated groups. All images were acquired using identical imaging parameters and scan settings. In each case, the intensities were normalized to 2 weeks post staggered injury in the rostral level. Student's t test; n = 3 sections per mouse and n = 3 mice per group. *$p < 0.05$ and ns, not significant. Error bar: SEM.

(C) The fluorescence intensity of mCherry and GFP immunostaining at 10 weeks post staggered injury in the vehicle treated and CLP290 treated groups. All images were acquired using identical imaging parameters and scan settings. In each case, the intensities were normalized to 2 weeks post staggered injury in rostral levels. Student's t test; n = 3 sections per mouse and n = 3 mice per group. *$p < 0.05$ and ns, not significant. Error bar: SEM.

(D) Schematic and images to show serotonergic axons in different levels of the spinal cord taken from 2 or 10 weeks after injury with or without CLP290 treatment.

(E and F) The fluorescence intensity of 5-HT immunostaining was compared at acute and chronic stages for vehicle treated groups (E), and also compared at chronic stages between vehicle and CLP290 treated groups (F). Student's t test; n = 3 sections per mouse and n = 3 mice per group. *$p < 0.05$ and ns, not significant. Error bar: SEM.

(G–I) (G) AAV-ChR2-GFP injected to the right cortex to trace CST axon terminations in different spinal cord levels in 2 or 10 week after injury with or without CLP290 treatment.

The fluorescence intensity of anti-GFP immunostaining was compared between acute and chronic stages in vehicle treated mice (H), and between vehicle or CLP290 treated groups at 10 weeks after injury (I). Scale bar: 100 μm. Student's t test; n = 3 sections per mouse and n = 3 mice per group. ns, not significant. Error bar: SEM.

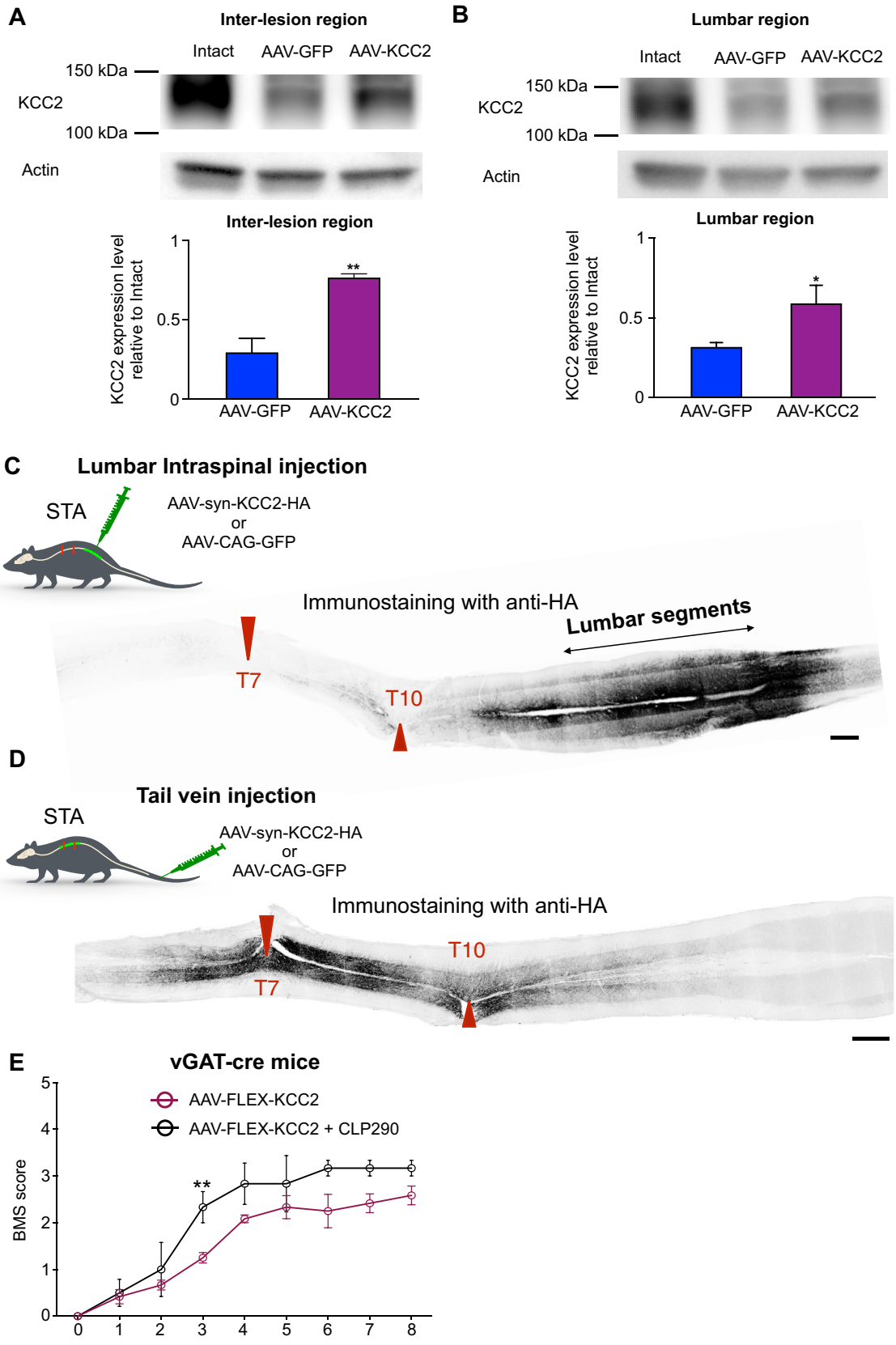

(legend on next page)

Figure S4. AAV-Mediated KCC2 Expression in Spinal Neurons and Its Behavioral Outcomes, Related to Figures 2 and 4

(A and B) Representative western blotting images and quantification showing KCC2 protein levels in the inter-lesion region (T8/9) (A) and in the lumbar spinal cord (L2-4) (B) of intact or stagger lesioned mice treated with either AAV-PHP.B-FLEX-GFP or AAV-PHP.B-HA-KCC2, at 10 weeks after injury. Actin as a loading control. n = 6, 5 and 5 mice for intact, AAV-PHP.B-GFP and AAV-PHP.B-HA-KCC2 group respectively. Student's t test; *$p < 0.05$; **$p < 0.01$; Error bars: SEM.

(C) Left, Schematic of experimental design. AAV virus was intraspinally injected into lumbar segments (L2-4) of experimental (AAV-1-Syn-HA-KCC2) and control mice (AAV-1-Syn-GFP-H2B). Right, representative confocal image stack of a longitudinal spinal cord section (from T5 to S1) at 10 weeks post staggered injury immunostained with anti-HA to label virally expressed KCC2.

(D) Left, Schematic of experimental design. AAV virus was injected into the tail vein of experimental (AAV-9-Syn-HA-KCC2) and control (AAV-9-Syn-GFP-H2B) mice. Right, representative confocal image stack of a longitudinal spinal cord section (from T5 to L3) at 10 weeks post staggered injury immunostained with anti-HA to label virally expressed KCC2. Scale bar: 500 μm.

(E) BMS scores measured at 24 hr in Vgat-Cre mice with tail vein injection of AAV-9-Syn-HA-KCC2 and treatment of vehicle or CLP290. Both groups started as n = 8, and at week 9 (the termination time point) n = 6 for both vehicle and CLP290 respectively. Repeated-measures ANOVA followed by post hoc Bonferroni correction. **$p < 0.01$; error bars, SEM.

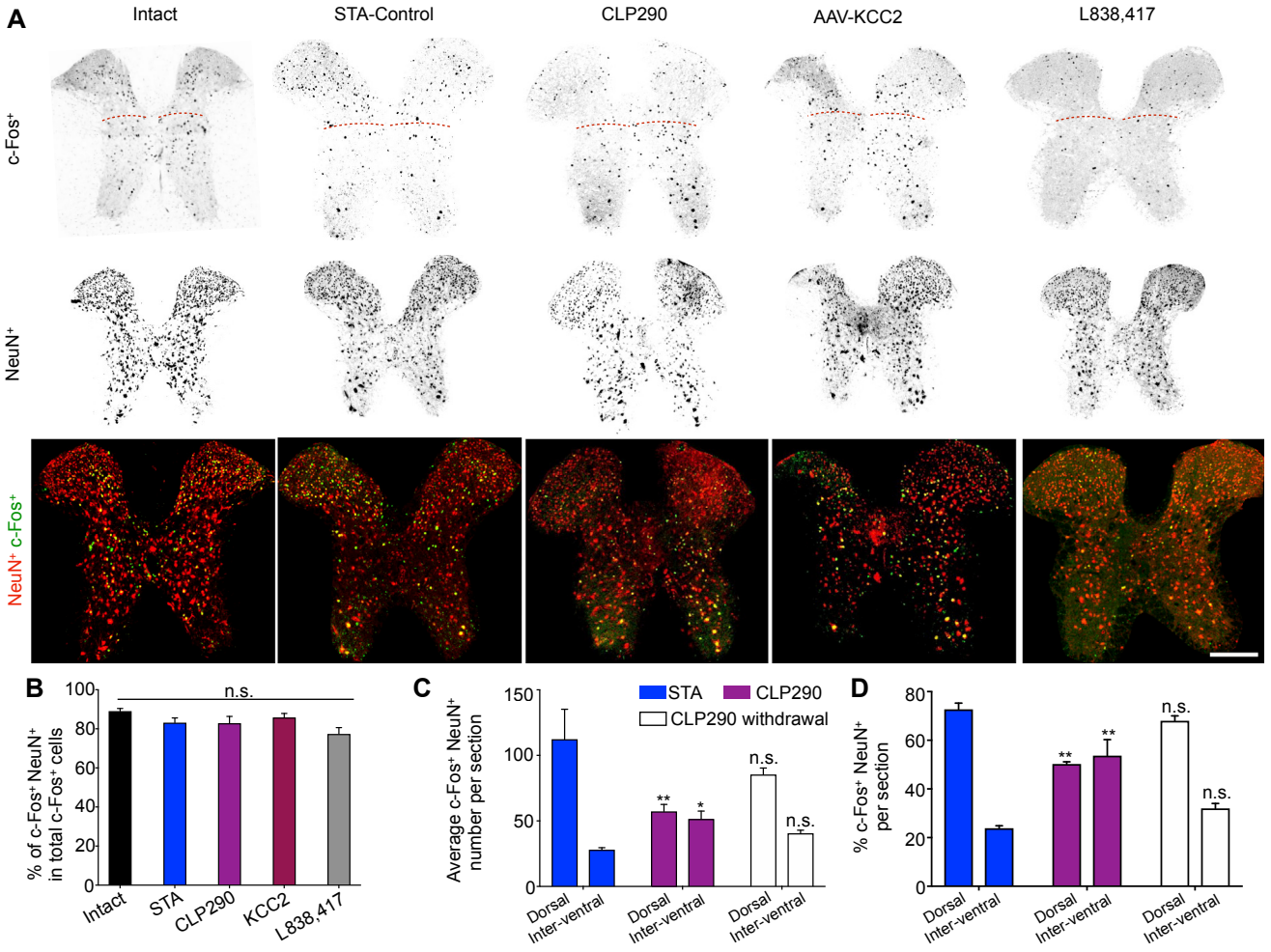

Figure S5. Altered c-Fos Expression Patterns in T8/9 of Stagger-Lesioned Mice with Different Treatments, Related to Figure 5

(A) Representative confocal image stacks of transverse sections from T8/9 spinal cord at 8 weeks after injury stained with antibody against c-Fos, NeuN or both c-Fos and NeuN. Scale bar: 100 μm.

(B) Percentages of NeuN$^+$ cells among c-*fos*$^+$ cells in intact mice or injured mice with individual treatments (vehicle control, CLP290, AAV-PHP.B-HA-KCC2 and L838,417). One-way ANOVA followed by Bonferroni post hoc test. n = 3 sections per mouse, n = 3 mice per group. n.s. not significant. Error bars: SEM.

(C) Average number of c-Fos$^+$ neurons per section in dorsal zone or in intermediate and ventral zones of staggered-lesioned mice with the treatment of vehicle (STA), continuous CLP290 treatment (CLP290), and 2 weeks after CLP290 withdrawal (CLP290 withdrawal). One-way ANOVA followed by Bonferroni post hoc test (c-Fos$^+$ NeuN$^+$ numbers of the dorsal or intermediate and ventral zones in the CLP290, or CLP290 withdrawal groups were compared to that of the vehicle group, respectively). n = 3 sections per mouse, n = 3 mice per group. *p < 0.05; **p < 0.01; n.s. not significant. Error bars: SEM.

(D) Average percentage of c-Fos$^+$ neurons per section in Laminae 1-5 or in Laminae 6-10 in staggered-lesioned mice with the treatment of vehicle (STA), continuous CLP290 treatment (CLP290), and 2 weeks after CLP290 withdrawal (CLP290 withdrawal). One-way ANOVA followed by Bonferroni post hoc test (c-Fos$^+$ NeuN$^+$ percentages of the dorsal or intermediate and ventral zones in the CLP290, or CLP290 withdrawal groups were compared to that of the vehicle group, respectively). n = 3 sections per mouse, n = 3 mice per group, **p < 0.01; n.s. not significant. Error bars: SEM.

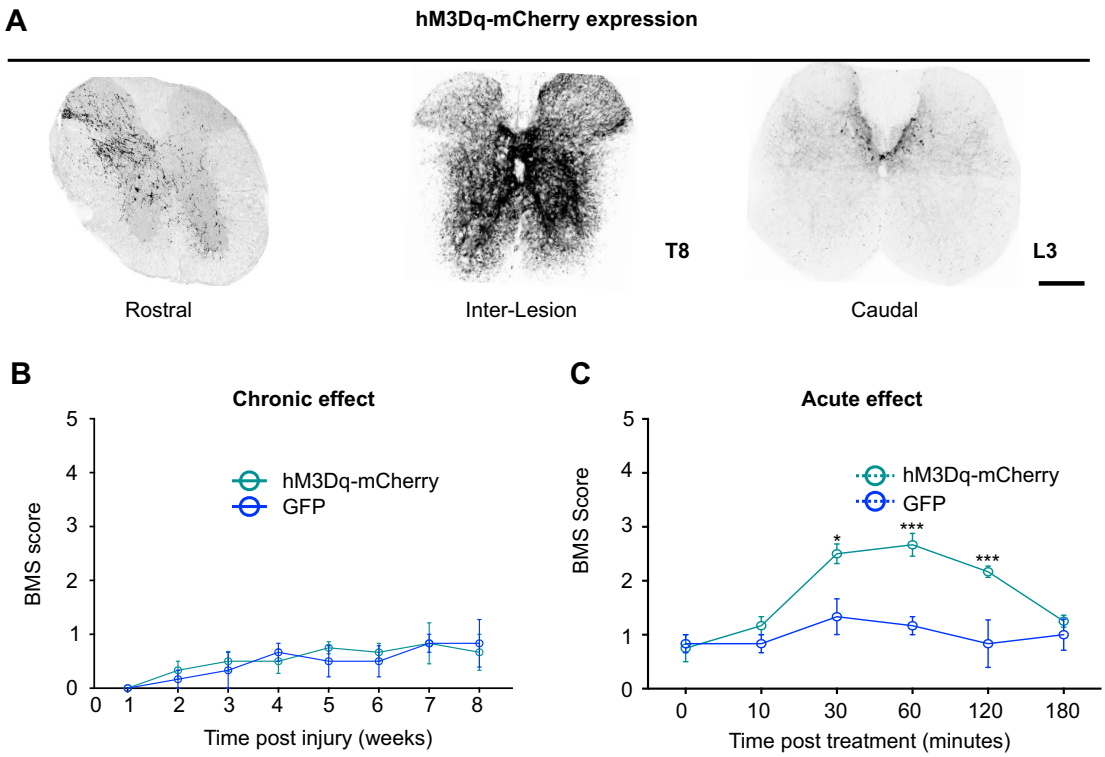

Figure S6. Gq-DREADD Expression in Spinal Excitatory Neurons Failed to Promote Functional Recovery in Stagger-Lesioned Mice, Related to Figure 6

(A) Representative confocal images of transverse sections of the thoracic and lumbar spinal cord at 8 weeks post staggered injury stained with anti-RFP to indicate hM3D DREADD expression. Scale bar: 100 μm.

(B) BMS scores of staggered injured Vglut2-Cre mice with viral injection of AAV9-Syn-FLEX-GFP or AAV9-FLEX-hM3Dq-mCherry. Repeated-measures ANOVA followed by post hoc Bonferroni correction. n = 5 for each group. Error bars: SEM.

(C) BMS scores measured acutely after compound treatments (10, 30, 60,120 and 180 min after CNO administration) in stagger-lesioned vGlut2-Cre mice at 8 weeks after SCI. Repeated-measures ANOVA followed by post hoc Bonferroni correction. n = 5, *$p < 0.05$; ***$p < 0.001$; error bars, SEM.